Low-temperature ordering in $YBa_2Cu_3O_{6+x}$ oxides at $x>0.5$: Computer simulation

S. Semenovskaya and A. G. Khachaturyan
Department of Materials Science, Rutgers University, P.O. Box 909, Piscataway, New Jersey 08855-0909
(Received 18 January 1996; revised manuscript received 7 May 1996)

Recent experimental data are used to formulate the effective pair interaction model of oxygen ordering in $YBa_2Cu_3O_{6+x}$ oxides at $x>0.5$ which is able to predict the main observed features of the low-temperature ordering. The computer simulation which uses this model characterizes the low-temperature secondary and tertiary ordering and describes the microstructure development resulting in formation of the Magneli-type and $2\sqrt{2}a_0\times 2\sqrt{2}a_0$ phases (a_0 is the perovskite lattice parameter). It is shown that these phases form stable rather than transient states. The stability fields of these phases on the phase diagram are estimated. Physical reasons distinguishing specific features of ordering in $YBa_2Cu_3O_{6+x}$ from the conventional ordering are discussed. The computer simulation results suggest certain heat treatment regimes which may provide formation of well-developed domains of the triple-period O-III and Magneli phases. The latter is important since lack of material with large domains poses a serious difficulty in experimental studies of these phases. [S0163-1829(96)02234-5]

I. INTRODUCTION

In spite of extensive experimental studies of oxygen ordering in the $YBa_2Cu_3O_{6+x}$ system, the physics of this ordering, strongly effecting the superconducting properties of these oxides, is still far from being well understood. In particular, the low-temperature ordering occurring within the stability field of the primary orthorhombic O-I ordered phase raises many questions which are still not answered. Even for the most thoroughly studied double-period $2a_0\times a_0$ or O-II secondary ordered phase, we still do not know why this phase does not coarsen into large ordered domains (the size of domains of this phase is usually so small and their superlattice diffraction maxima at {(1/2)00} points are so weak and diffuse that most of the researches call the O-II ordered phase a short-range order state). We still do not know whether the O-II phase transforms to other ordered phases upon cooling or these phases are formed by different mechanism.

The triple-period $3a_0\times a_0$ (O-III) ordered phase and other Magneli-type[1] long-period phases $na_0\times a_0$ (where integer $n>2$) which are also observed in this system are understood even less. With the exception of the O-III phase, the $na_0\times a_0$ phases were observed only occasionally and only by the electron microscopy methods. These phases, like the O-II phase, also do not coarsen during ordering and produce very weak diffuse diffraction maxima. It is not clear whether the $na_0\times a_0$ ordered states are really the stable phases characterized by the corresponding stability fields on the phase diagram or they are just transient states formed along the transformation path. If these phases are stable at certain temperatures T and stoichiometries x, then the question is what kind of the thermal treatment is required to facilitate their formation and growth.

The most controversial problem is the origin of the so-called $2\sqrt{2}a_0\times 2\sqrt{2}a$ ordered phases with the $\sqrt{2}a_0\times 2\sqrt{2}a$ and $2\sqrt{2}a_0\times 2\sqrt{2}a$ unit cells. At $x>0.5$, these phases were also observed only occasionally and only by electron microscopy methods.[2–4] It is unclear why these phases produce sharp and strong {(1/4)(1/4)0}-type diffraction maxima on the diffraction pattern while the diffraction maxima of the main secondary ordered O-II phase are weak and diffuse. Since most of studies reported the observation of the $\sqrt{2}a_0\times 2\sqrt{2}a_0$- or $2\sqrt{2}a_0\times 2\sqrt{2}a_0$-type phases within the ''tetragonal'' nonsuperconducting range $x<0.4$,[5–13] the very fact of formation of the $2\sqrt{2}a_0\times 2\sqrt{2}a$ ordered phases at $x>0.5$ is still debated.

Some advance in understanding the oxygen-ordering phenomena in the $YBa_2Cu_3O_{6+x}$ system at $x<0.4$ (nonsuperconducting region) was achieved in our previous work.[14] It was shown that, contrary to the O-Cu-O [010] chain $na_0\times a_0$ superstructures formed at $x>0.4$, the $\sqrt{2}a_0\times 2\sqrt{2}a_0$ phases at $x<0.4$ are formed by alternating oxygen atoms chains along the ⟨110⟩ directions. However, the problems of the low-temperature secondary and tertiary ordering in the superconducting range $x>0.4$–0.5 were not addressed in Ref. 14.

The purpose of this study is an attempt to fill this gap and to answer the above-mentioned questions concerning the low-temperature ordering in the $YBa_2Cu_3O_{6+x}$ system at $x>0.4$–0.5. This task turns out to be possible only because of availability of new experimental data[15–17] at $x>0.4$–0.5 (on the temperature T_2 of the O-I→O-II transition,[15,16] on the shape of the {(1/2)00} diffuse maxima,[15,17] and the observation of the O-III phase at certain thermal treatments).[16] The use of these data allowed us to formulate a more realistic interaction model of the effective long-range O-O pair interaction. The very procedure of finding the O-O interaction potential is such that the computer simulation performed with this potential reproduces the experimental data[15–17] to which it is fitted. However, the computer simulation also fairly well reproduces and explains many other phenomena observed at the low-temperature ordering. Unlike previous models, the proposed model is able to obtain practically all major observed structural features of the low-temperature ordering and characterize the thermodynamic properties of the ordered phases.

The analysis of the simulated microstructures and their diffraction patterns at different stoichiometries x and tem-

peratures T and the microstructure evolution have shown that (i) all low-temperature phases, O-II, O-III, Magneli, and $2\sqrt{2}a_0\times 2\sqrt{2}a_0$, are the stable phases characterized by the stability fields on the phase diagram; (ii) the oxygen atom interaction used in this work simultaneously describes the formation of two groups of phases of very different natures, the $na_0\times a_0$ and $2\sqrt{2}a_0\times 2\sqrt{2}a_0$ phases which are formed at different x and T; (iii) the simulation results enable us to propose the thermal treatment regimes facilitating formation of the low-temperature ordered phases which are not obtainable by a regular slow cooling.

The computer simulation also shows that the low-temperature ordering is very sensitive to the O-O interaction. We note that the previously suggested O-O potential,[18–22] which was estimated when new experimental data[15–17] were not available, gave only the O-II and $2\sqrt{2}a_0\times 2\sqrt{2}a_0$ phases. It could not describe all observed phases including, beside the O-II phase and $2\sqrt{2}a_0\times 2\sqrt{2}a_0$, the O-III and Magneli phases.

II. EXPERIMENTAL DATA

Below we briefly describe new experimental data[15–17] which we used to formulate a more realistic O-O interaction model for the computer simulation of the low-temperature oxygen ordering. This ordering occurs at temperatures below the temperature T_0 of the primary ordering $T\rightarrow$O-I transition, where the orthorhombic primary ordered phase O-I forms from the tetragonal disordered phase T.

A. O-II double-period phase

In a neutron diffuse scattering study,[15] the intensity of the superlattice {(1/2)00} diffuse maxima of the O-II phase was measured at different temperatures in single crystals with the oxygen composition x within the range $0.5<x<0.68$. It was found that the transition temperature T_2 of the secondary O-I→O-II ordering is practically independent on x. The observed constant value $T_2\approx 150$ °C is considerably less than the value $T_2\sim 450$ °C used in our previous estimates of the O-O potential.[18–22]

The temperature T_2 for a larger interval $0.5<x<0.8$ was also estimated by Yang *et al.*[16] who studied the superconducting transition temperature T_c after different heat treatments. This study showed a remarkable change in the relaxation behavior of T_c caused by oxygen ordering. This behavior depends on whether the samples were quenched from above or from below the threshold temperature T^* which was associated with the onset of the O-I→O-II transition. Since the authors observed the diffraction from the triple-period O-III ordered phase at $x=0.65\sim 2/3$, they assumed that at $x\geqslant 2/3$ the temperature T^* may be associated with a more complex ordering involving the O-III phase as well. The values of T^* reported in Ref. 16 are slightly higher than the temperature $T_2\sim 150$ °C∼const observed in Ref. 15 and T^* depends on x ($T^*\approx 170$ °C for $x\sim 0.65$, 160 °C for $x\sim 0.72$, and 210 °C for $x\sim 0.82$).

The neutron-diffraction single-crystal studies[15,17] reported the observation of a specific shape of the prototype {(1/2)00} diffuse maxima of the O-II phase. It was found that these maxima have a nearly perfect ''elliptic'' shape for the well-annealed samples with $x\sim 0.55$ (Ref. 15) and $x\sim 0.40(5)$.[17] The long axis of the ellipse is parallel to the a axis (perpendicular to the Cu-O chains) whereas the short axis is parallel to the b axis (parallel to the Cu-O chains). The anisotropy of the maxima is determined by the ratio of the axes of the ellipse which is equal to ∼2.5 (the same anisotropy was reported in Ref. 15 for a sample with $x\sim 0.50$).

Our analysis of computer-simulation data has shown that the anisotropy of {(1/2)00} diffuse maxima imposes a strong constraint on possible values of O-O interaction energies. Therefore, the diffuse scattering data[15,17] give important information which we use (together with data[15,16] on the transition temperatures) for the formulation of a more realistic oxygen interaction model.

B. O-III triple-period phase

Reliable information on the triple-period O-III ordered phase was obtained in the electron diffraction study[16] using a special energy filtering technique and x-ray diffraction study[23] (the O-III phase was also observed in Refs. 4 and 7). In single crystals with $x=0.65\sim 2/3$, the {(1/3)00}-type diffuse maxima of the O-III phase were observed after different quenching and annealing treatments.[16] It was found that the intensities of these maxima are of the same order of magnitude as the intensities of the {(1/2)00}-type maxima observed in the stoichiometric O-II phase (at $x\sim 0.5$) with use of the same technique.[16] It is important that practically only the {(1/3)00}-type diffraction maxima were observed in crystals with $x\gtrsim 2/3$.[16,23] These observations showed that at $x\gtrsim 2/3$ and $T\sim T_{\rm room}$ the O-III phase is a more stable phase than the O-II phase.

Our computer simulation and qualitative physical arguments (given in the Discussion) indicate that the O-III phase cannot be formed in the O-II→O-III transition. It forms only as a result of the O-I→O-III ordering. Study of the O-III phase,[16] obtained in different quenching-annealing experiments, allows us to estimate the temperature $T_{\rm III}$ of the O-I→O-III ordering transition. In Ref. 16, an almost pure O-III phase at $x=0.65\sim 2/3$ was produced in either one of two treatments: (i) after quenching the thermally equilibrated samples from the temperature $T_{\rm quen}=259$ °C to $T_{\rm room}$, (ii) after annealing for one week at $T_{\rm ann}=120$ °C (samples were previously quenched from 520 °C to the liquid nitrogen[16,24]); the annealing at 120 °C has been followed by a ''stepped cool-down to room temperature'' $T_{\rm room}$.

It is clear that the quenching temperature $T_{\rm quen}=259$ °C in treatment (i) is within the O-I phase stability field because $T_{\rm quen}$ is higher than the observed temperature $T^*\sim T_2\sim 170\ ^\circ C$ (Ref. 16) of the O-I→O-II transition in this sample. Therefore, since this quenching to the room temperature $T_{\rm room}$ produces the O-III phase, this means that $T_{\rm room}$ is located within the stability field of the O-III phase, i.e., $T_{\rm room}<T_{\rm III}$.

The fact that the O-III phase cannot be formed in the O-II→O-III transition indicates that the annealing temperature $T_{\rm ann}=120$ °C [treatment (ii) producing the O-III phase] is within the stability field of the O-III phase. Otherwise, if the temperature $T_{\rm ann}=120$ °C were within the O-II phase stability field, this annealing would produce the O-II phase which cannot transform to the O-III phase. The observation of the O-III phase[16] contradicts this scenario. Therefore, ob-

servation of the O-III phase in thermal treatments (i) and (ii) provides the following estimate for the temperature T_{III} of the O-I→O-III transition:

$$120\ ^\circ C < T_{III} < T^* \sim 170\ ^\circ C. \quad (1)$$

C. Magneli-type and $2\sqrt{2}a_0 \times 2\sqrt{2}a_0$ phases

There are several studies reporting the observation of the long-period Magneli-type phases with a $(2n+1)a_0 \times a_0$ unit cell (n is an integer).[4,7,23,25,26] The stoichiometries of these phases described by the formula $YBa_2Cu_3O_{7-n/(2n+1)}$ were predicted by one of the authors.[1] The corresponding values of x are $x=(n+1)/(2n+1)$, i.e., 2/3, 3/5, 4/7, and so on. These phases can be detected from their diffraction patterns containing weak diffuse maxima in the superlattice positions $[n/(2n+1)00]$: [(1/3)00], [(2/5)00] and [(3/7)00] and so on.[4,7,16,23,25,26] The first and more regularly observed member of this Magneli series corresponds to $n=1$. It is the O-III phase with a $3a_0 \times a_0$ unit cell.[4,7,16,23,26] This phase is the most stable member of this Magneli series because it is generated by the the superlattice vectors belonging to the only star and, thus, it meets the maximum structure amplitude requirement.[27] The O-III phase is characterized by the {(1/3)00}-type superstructure maxima.

The next member of the family is labeled by the number $n=2$. It is the O-V phase with a $5a_0 \times a_0$ unit cell. It generates weak superlattice maxima at [(2/5)00] and [(3/5)00] points which were occasionally observed on electron-diffraction patterns[7,25,26] (the images of small patches of this [(2/5)00] Magneli phase were obtained by TEM in Ref. 7). Available experimental data show that this structure consists of very small microdomains which do not coarsen during ordering.

A different type of oxygen ordering is presented by the $2\sqrt{2}a_0 \times 2\sqrt{2}a_0$ ordered phases. They generate a totally different type of diffraction pattern, with strong and sharp {(1/4)(1/4)0}-type diffraction maxima. These diffraction patterns were found in electron-diffraction studies [for $x \sim 0.85$ (Refs. 2 and 3) and $x \sim 0.64$ (Ref. 4)]. However, in majority of studies, a similar type of diffraction pattern, with the strong and sharp {(1/4)(1/4)0}-type and {(1/2)(1/2)0} diffraction maxima, was found in samples having much smaller oxygen composition $x<0.4$, i.e., within the nonsuperconducting range of stoichiometry. In spite of the results,[2–4] there is still no consensus on whether the {(1/4)(1/4)0} phases are really formed at larger $x>0.5$ or their observations were caused by inhomogeneity in oxygen composition.

In our previous studies,[19,20,22] it was shown that the $2\sqrt{2}a_0 \times 2\sqrt{2}a_0$ phases, producing the {(1/4)(1/4)0}-type maxima on diffraction patterns, could be formed at $x>0.5$. In this case they are formed from the O-II phase in the tertiary ordering transition O-II→$2\sqrt{2}a_0 \times 2\sqrt{2}a_0$.

Although these observations of Magneli-type and $2\sqrt{2}a_0 \times 2\sqrt{2}a_0$ phases do not give a specific quantitative information (for example, values of transition temperatures) that can be used for fitting the O-O interaction energies, however they are also important since any realistic O-O interaction energies have to satisfy these observations.

III. THE O-O INTERACTION MODEL

To describe the oxygen ordering in the $YBa_2Cu_3O_{6+x}$ system at $x>0.5$, we used the same approach to formulating the O-O interaction model as that employed in our previous work for the range $x<0.4$.[14] The effective O-O pair-interaction energies between O atoms at the interstitial sites $(p,\mathbf{r})$ and $(q,\mathbf{r}')$ are described by the function $W(\mathbf{r}-\mathbf{r}')_{pq}$ where $(p,\mathbf{r})$ and $(q,\mathbf{r}')$ are the coordinates of sites occupied by O atoms, $\mathbf{r}$ is the translation vector labeling the origin of unit cell in a (001) Cu(1)-O basal plane [the position of a Cu(1) atom in our case] and the index p $(p,q=1,2)$ is the type of an interstitial site within this unit cell (the type of the interstitial site sublattice). According to the concentration wave approach,[28,29] the stability of ordered structures is determined by the minima of the eigenvalues of the Fourier transforms of $W(\mathbf{r})_{pq}$:

$$V(\mathbf{k})_{pq} = \sum_{\mathbf{r}} W(\mathbf{r})_{pq} \exp(-i\mathbf{kr}), \quad (2)$$

where $\mathbf{k}$ is the wave vector defined within the first Brillouin zone of a disordered phase. Since $p,q=1,2$, the function $V(\mathbf{k})_{pq}$ is a Hermitian 2×2 matrix. Therefore, this matrix has two branches of real eigenvalues, $\lambda(\mathbf{k})_{\pm}$. The structure of a stable ordered phase is determined by the minimum value of the eigenvalues belonging to the lower branch $\lambda(\mathbf{k})_{-}$. The star of the vector $\mathbf{k}$ providing the minimum of $\lambda(\mathbf{k})_{-}$ generates the stable ordered phase.

By definition, the spectrum $\lambda(\mathbf{k})_{-}$ has extrema at all of the Lifshitz points in the first Brillouin zone of a disordered phase, irrespective of the choice of the potential $W(\mathbf{r})_{pq}$. For $YBa_2Cu_3O_{6+x}$, these Lifshitz points defined in the first Brillouin zone of the disordered tetragonal T phase are determined by the vectors $\mathbf{k}_0=(2\pi/a_0)(000)$, $\mathbf{k}_1=(2\pi/a_0)[(1/2)00]$ and $\mathbf{k}_2=(2\pi/a_0)[(1/2)(1/2)0]$. They generate three basic superstructures. The further secondary and tertiary ordering of nonstoichiometric oxygen vacancies within these basic superstructures produces the corresponding derivative superstructures upon cooling. The vectors $\mathbf{k}_0$ and $\mathbf{k}_1$ corresponding to the eigenvalues $\lambda(000)_{-}$ and $\lambda[(1/2)00]_{-}$ are responsible for formation of O-I and O-II parent superstructures. The $3a_0$ or O-III phase and other $(na_0 \times a_0)$ Magneli-type phases are their derivatives. Together they form a group of O-Cu-O [010] chain structures observed at $x>0.4$.

The vector $\mathbf{k}_2$ and the eigenvalue $\lambda[(1/2)(1/2)0]_{-}$ are responsible for formation of the primary ordered phase, characterized by the superlattice vector $\mathbf{k}_2=(2\pi/a_0)[(1/2)(1/2)0]$. Its derivatives formed by the secondary and tertiary ordering are the $\sqrt{2}a_0 \times 2\sqrt{2}a_0$ superstructures observed at $x<0.4$. These structures are formed as alternating oxygen-atom chains in ⟨110⟩ directions.[14]

The effective O-O pair-interaction potential $W(\mathbf{r}-\mathbf{r}')_{pq}$ consists of two parts: the anisotropic screened-Coulomb part $W(\mathbf{r}-\mathbf{r}')^{f}_{pq}$ and the strain-induced interaction part $W(\mathbf{r}-\mathbf{r}')^{\text{elast}}_{pq}$ (both parts are defined as in Ref. 14):

$$W(\mathbf{r}-\mathbf{r}')_{pq} = W(\mathbf{r}-\mathbf{r}')^{f}_{pq} + W(\mathbf{r}-\mathbf{r}')^{\text{elast}}_{pq}. \quad (3)$$

Equations which we used to calculate the Fourier transforms of the strain-induced interaction $W(\mathbf{r}-\mathbf{r}')^{\text{elast}}_{pq}$ are presented in the Appendix. The anisotropic screened-Coulomb potential $W(\mathbf{r}-\mathbf{r}')^{f}_{pq}$ in Eq. (3) is

$$W(\mathbf{r}-\mathbf{r}')^{f}_{pq}=\begin{cases}\dfrac{(z^*)^2}{r_i}\exp\left(-\dfrac{r_i}{r_D}\right)+\delta W_i & \text{at } i\neq 2 \text{ for } |\mathbf{r}-\mathbf{r}'|\neq a_0,\\ (1\pm f)\dfrac{(z^*)^2}{a_0}\exp\left(-\dfrac{a_0}{r_D}\right)+\delta W_2 & \text{at } i=2 \text{ for } |\mathbf{r}-\mathbf{r}'|=a_0,\end{cases} \tag{4}$$

where r_i is the radius of the O-O ith coordination shell, z^* is effective oxygen charge including the dielectric constant, r_D is the screening radius, f is the anisotropy factor for the next-nearest-neighbor interaction ($i=2$) which is used with the sign $(-)$ for the O-O interaction across a Cu atom and with the sign $(+)$ otherwise; δW_i is the correction to the screened-Coulomb interaction in the ith oxygen coordination shell which is due to the spatial dispersion of the dielectric constant.

We note that for $i=2$ (next-nearest oxygen atoms) Eq. (4) includes two types of corrections to the screened-Coulomb asymptotic: δW_2 and the term proportional to the anisotropy factor $\pm f$. Only the latter correction was considered in theoretical studies[30–33] [these studies did not take into account the corrections δW_i to other coordination shells and ignored the strain-induced interaction $W(\mathbf{r}-\mathbf{r}')^{\text{elast}}_{pq}$].

A. Transition temperatures

Experimental results[15,16] described in Sec. II provide the values of the transition temperature T_2 of the O-I→O-II transition and also the estimate of the temperature T_{III} of the O-I→O-III transition [see Eq. (1)].

The concentration wave approach[28,29] allows one to describe the ordered structures and the corresponding transition temperatures in terms of the Fourier transforms $V(\mathbf{k})_{pq}$ [Eq. (2)] of the interaction energies $W(\mathbf{r})_{pq}$. In particular, the transition temperatures T_2 and T_{III} are related to the interaction energies by the equations

$$T_2=-\frac{2c(1-2c)}{k_B}V_{22}(\tfrac{1}{2}00), \tag{5a}$$

$$T_{\text{III}}=-\frac{2c(1-2c)}{k_B}V_{22}(\tfrac{1}{3}00), \tag{5b}$$

where k_B is the Boltzmann constant and $2c=x$ is oxygen stoichiometry. Equations (5a) and (5b) are derived under the assumption that the primary O-I orthorhombic phase is almost completely ordered at the moment when the secondary ordering occurs. The latter means that there are no O atoms at the positions on the a axis and all O atoms occupy positions at the b axis. A similar equation for the temperature T_0 of the T→O-I transition has the form

$$T_0=-c(1-c)\lambda(000)_-/k_B$$
$$=-\frac{c(1-c)}{k_B}[V_{11}(000)-|V_{12}(000)|]. \tag{5c}$$

Equations (5) allow one to find the Fourier components $V(\mathbf{k})_{pq}$ of the O-O interaction potential $W(\mathbf{r}-\mathbf{r}')_{pq}$ for the superlattice vectors $\mathbf{k}_j$ of the O-II, O-III, and O-I phases, $\mathbf{k}_1=(2\pi/a_0)[(1/2)00]$, $\mathbf{k}_3=(2\pi/a_0)[(1/3)00]$, and $\mathbf{k}_0=(2\pi/a_0)(000)$, respectively, from the experimentally observed transition temperatures T_2, T_{III} and T_0 (for $x\sim 0.5$ the transition temperature $T_0\sim 970$ K was found in Ref. 34). Therefore, the O-O interaction potential should be chosen so that the Fourier transforms $V_{22}(\mathbf{k}_j)$ and $\lambda(000)_-$, calculated with this potential and used in Eq. (5) give the observed temperatures T_2, T_{III} and T_0.

It should be noted that Eqs. (5) are derived within the mean-field approximation which is a reasonable approximation for the relevant case of the long-range interaction. The O-O interaction potentials used in all existing theories of ordering in $YBa_2Cu_3O_{6+x}$ are the effective pair potentials. Their use provides the simplest description of the system thermodynamics. As for the O-O potentials obtained by comparison of observed values with the corresponding calculated mean-field values [particularly, by comparison of observed ordering temperatures with the mean-field ones given by Eqs. (5)], they are in fact the *effective mean-field potentials*. These potentials are actually very good for calculations of other independent characteristics of a system, especially for systems with the second-order transitions. The latter has been particularly illustrated by one of the authors.[35] It was shown in Ref. 35 that a quite complicated phase diagram of the Fe-Al alloys with a multitude of ordering reactions is very well described by the mean-field theory whose effective mean-field potentials are found from comparison of the mean-field equation for the diffuse scattering with the observed values of the diffuse scattering.

For the $YBa_2Cu_3O_{6+x}$ system the transition sequence

$$T\rightarrow \text{O-I}\rightarrow \text{O-II}, \tag{6}$$

observed at cooling the tetragonal T phase within the superconducting range $x>0.4$, requires that the main eigenvalues $\lambda(\mathbf{k}_j)_-$ should meet the following inequalities:[14,19,20]

$$\lambda(000)_-<\lambda[\tfrac{1}{2}00]_-=V_{22}(\tfrac{1}{2}00)<\lambda(\tfrac{1}{2}\tfrac{1}{2}0)_-=V_{22}(\tfrac{1}{2}\tfrac{1}{2}0). \tag{7}$$

[In Eq. (7), the conditions $V_{12}[(1/2)00]=V_{12}[(1/2)(1/2)0]=0$ following from the symmetry of the O-I phase are taken into account.] The other requirement is that the potential should provide negative minima of $\lambda(\mathbf{k}_j)_-$ at the corresponding Lifshitz points $\mathbf{k}_0$, $\mathbf{k}_1$, and $\mathbf{k}_2=(2\pi/a_0)[(1/2)(1/2)0]$.

B. Dependence of $V_{22}[(1/2)00]$ on oxygen stoichiometry x

Figure 1 shows the values of the Fourier transform $V_{22}[(1/2)00]$ for the stoichiometries $x=0.5$, 0.57, 0.6, and 0.64 which we found by equating the transition temperature T_2 given by Eq. (5a) to the observed values of $T_2\approx 423$ K (150 °C) at these stoichiometries.[15] It also presents the values of $V_{22}[(1/2)00]$ found from the transition temperatures

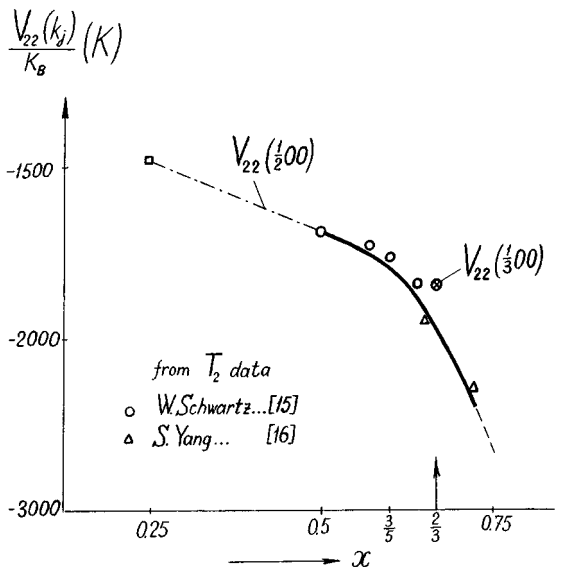

FIG. 1. The dependence of the Fourier transform $V_{22}[(1/2)00]=\lambda[(1/2)00]_-$ of the O-O interaction potential on the stoichiometry x. It is found from the observed temperatures T_2 of the O-I→O-II transition (Refs. 15 and 16) and the mean-field equation (5a). The circles represent the values of $V_{22}[(1/2)00]$ following from the constant temperature $T_2\sim150$ °C$\sim$const (Ref. 15), the triangles, from the temperatures $T^*\sim T_2$ obtained in Ref. 16. The solid line represents the averaged stoichiometry dependence which is used in this paper. The value $V_{22}[(1/2)00]/k_B\sim1480$ K at $x\sim0.25$ is found in Ref. 14. An encircled cross indicates the value of $V_{22}[(1/3)00]$ at the superlattice point $\mathbf{k}_3=(2\pi/a_0)[(1/3)00]$ of the O-III phase estimated in this work from the experimental data (Ref. 16) at $x=0.65\sim2/3$ [see Eq. (8a)].

$T_2\sim T^*\sim170$ °C ($x\sim0.65$) and ~160 °C ($x\sim0.72$) obtained in Ref. 16 (shown by triangles). For the estimate of the O-O interaction potential, we use the dependence of $V_{22}[(1/2)00]$ on x averaged over both data[15,16] which is shown on Fig. 1 by a solid line. This dependence reflects the change in T_2 within the interval 150 °C$\leqslant T_2\leqslant$163 °C. Figure 1 also presents the value $V_{22}[(1/2)00]/k_B=\lambda[(1/2)00]_-/k_B\approx-1480$ K found in Ref. 14 for $x\sim0.25$.

Figure 1 demonstrates that the Fourier transform $V_{22}[(1/2)00]$ noticeably changes with the stoichiometry x. This figure also presents the estimated value of the Fourier transform $V_{22}[(1/3)00]$ for the superstructure vector of the O-III phase, $\mathbf{k}_3=(2\pi/a_0)[(1/3)00]$, at $x\sim2/3$ (shown by encircled cross). This value

$$V_{22}(\tfrac{1}{3}00)/k_B\sim-1840\ \ (\mathrm{K}) \tag{8a}$$

used for fitting the O-O interaction potential and analysis of O-III phase ordering follows from the relation

$$-1768\ \ (\mathrm{K})>V_{22}(\tfrac{1}{3}00)/k_B>-1963\ \ (\mathrm{K}) \tag{8b}$$

which, in turn, follows from Eqs. (1) and (5b). Using this value of $V_{22}[(1/3)00]$ in Eq. (5b) results in the transition temperature $T_{\mathrm{III}}\sim136$ °C satisfying Eq. (1).

Figure 1 illustrates that at $x\sim2/3$ (and certainly at $x<2/3$)

$$V_{22}(\tfrac{1}{2}00,x)<V_{22}(\tfrac{1}{3}00,x). \tag{9}$$

This relation follows from $T_{\mathrm{III}}<T_2$ and Eqs. (5a) and (5b). The condition $T_{\mathrm{III}}<T_2$, in turn, follows from the numerous observations of the O-I→O-II ordering rather than the O-I→O-III ordering within the range $0.4\leqslant x\leqslant0.64$ (see, for example, Refs. 15 and 16). We also assume that relation (9) holds at the slightly larger stoichiometry $x\sim2/3>0.64$. Indeed, if the contrary condition, $V_{22}[(1/2)00,x]>V_{22}[(1/3)00,x]$, is assumed at $x\sim2/3$, then the O-I→O-III ordering should occur even at slow cooling and, therefore, the O-III phase would always be more stable than O-II phase at all temperatures and stoichiometries around $x\sim2/3$. It would be observed as commonly at its stoichiometry $x\sim2/3$ as the O-II phase at its stoichiometry $x\sim1/2$. However, this is not the case. The O-III phase was observed only after special thermal treatments[16,23] and not after a regular slow cooling of the O-I phase.

C. Estimation of the O-O potentials

The strain energy contribution to the O-O potential (3) was estimated using Eqs. (A1)–(A5). The anisotropic screened-Coulomb potential (4) is determined by the parameters δW_i, f, z^* and r_D which are estimated at different compositions x by fitting them to the values of $V_{22}[(1/2)00]$, $V_{22}[(1/3)00]$, and $\lambda(000)_-$. The latter were determined from the observed transition temperatures T_2,[15,16] T_{III},[16] and T_0 (Ref. 34) by using Eqs. (5) [see also Eq. (8a) and Fig. 1]. The additional condition that the microstructure of the O-II phase simulated with these parameters should generate the diffraction pattern with the {(1/2)00} diffuse maxima of the same shape as that observed in Refs. 15 and 17 was also used. This shape of the maxima is an ellipse extended in the [100] direction with the ratio of principal axes close to 2.5.

The parameters δW_i, f, and z^* found from this fitting procedure are shown in Fig. 2. They are used in our computer simulation. The screening radius $r_D=4a_0/\sqrt{2}$ is chosen to be the same as in Ref. 14. The parameters δW_i, f, and z^* at $x\sim0.25$, found in Ref. 14 by utilizing exactly the same procedure, are also shown in Fig. 2. An important conclusion following from the results presented in Fig. 2 is that the corrections δW_i to the screened-Coulomb potential comparatively rapidly decay with the O-O separation distance r_i. Although the corrections were estimated up to the distance corresponding to the radius of the seventh coordination shell, only the first five of them have a significant value. Vanishing of corrections for $r>r_5$ is actually an independent indication that the chosen potential $W(\mathbf{r})^f_{pq}$ [Eq. (4)] at large distances r is reasonably well described by the screened-Coulomb long-range asymptote with $r_D=4a_0/\sqrt{2}$. Figure 2 also demonstrates that the parameters δW_i depend on the stoichiometry. This dependence is significant between $x\sim0.25$ and $x\sim0.5$, i.e., around the critical composition $x_{\mathrm{cr}}\sim0.35$–0.4 where the material changes its conductivity from the superconducting to the semiconducting type. Some dependence of δW_i from x still exists at $x>0.5$, though it is much less pronounced.

For $x>0.4$–0.5, Fig. 2 presents only the values δW_2, δW_3, δW_5, and δW_7 related to the O-O pairs located in the same sublattice. This is because of the fact that the secondary and tertiary ordering in the nonstoichiometric O-I phase develops due to oxygen atom rearrangements within the only sublattice and therefore the experimental data[15–17] on this

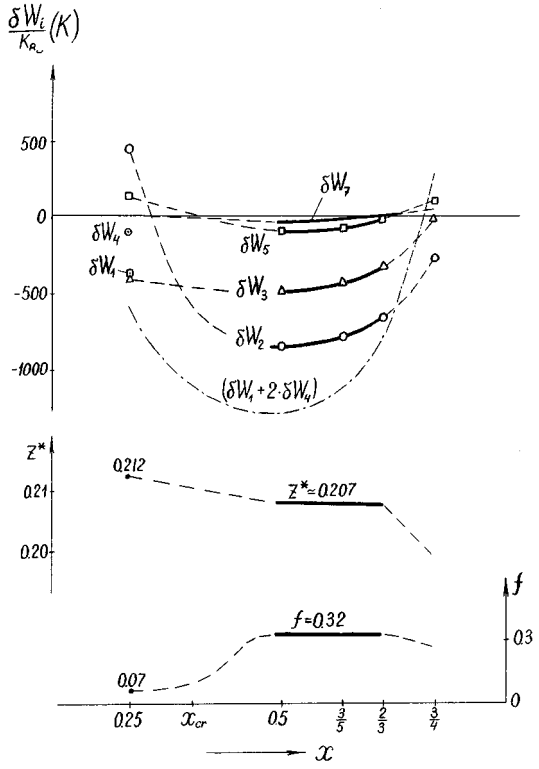

FIG. 2. Estimated values of the parameters of the anisotropic screened-Coulomb potential [Eq. (4)] at $x>0.5$: the corrections δW_i, the effective oxygen ions charge z^* (in units of the electron charge) including the dielectric constant, and the anisotropy factor f for the next-nearest intersite distance ($i=2$). The values of the parameters for $x\sim 0.25$ are found in Ref. 14. The screening radius $r_D=4a_0/\sqrt{2}$. The parameters for $x>0.5$ are found by fitting to the experimental data (Refs. 15–17). Dashed-line segments at $x>2/3$ indicate the extended parts of the corresponding dependences which are not covered by experimental data (Refs. 15–17).

type of ordering can give information only about the O-O interaction within this sublattice. The parameters δW_1, δW_4, δW_6,... related to the O-O pairs located in different sublattices can be found from experimental data on ordering involving oxygen atom transitions between different sublattices. For example, the experimental value of the temperature T_0 of the $T\rightarrow$O-I transition provides the value $\lambda(000)_-=V_{11}(000)-|V_{12}(000)|$ [see Eq. (5c)] which, in turn, for $x>0.4$, gives the sum $(\delta W_1+2\delta W_4+\delta W_6)\sim(\delta W_1+2\delta W_4)$. Its values are presented in Fig. 2.

Figure 2 demonstrates that the main change with stoichiometry x, when it increases from $x<x_{\rm cr}$ to $x>x_{\rm cr}$, occurs for the corrections related to the next-nearest oxygen atoms: the anisotropy factor f (favoring the formation of the O-Cu-O [010] chains) and δW_2. The effective oxygen charge z^*, including the dielectric constant, is given in units of the electron charge. It practically does not change within the range $0.25<x<2/3$.

IV. COMPUTER-SIMULATION METHOD

The computer simulation of the diffusion kinetics of oxygen ordering is based on the improved stochastic version of the microscopic crystal lattice site diffusion equation used in Refs. 14 and 18–22. The stochastic equation includes the random noise term simulating thermal fluctuations. This stochastic version of the microscopic diffusion kinetic equations, which, in fact, is the discrete Langevin equation, has a form

$$\frac{dn_p(\mathbf{r},t)}{dt}=\sum_{q=1}^{q=2}\sum_{\mathbf{r}'}L(\mathbf{r}-\mathbf{r}')_{pq}\frac{\delta F}{\delta n_q(\mathbf{r}',t)}+\xi_p(\mathbf{r},t), \tag{10}$$

where $n_p(\mathbf{r},t)$ is the occupation probability to find an oxygen atom at the site $(p,\mathbf{r})$ at time t, the site coordinates $(p,\mathbf{r})$ are defined in the comment to Eq. (2), summation over $\mathbf{r}'$ is carried out over all N unit cells of the crystal. The function $L(\mathbf{r}-\mathbf{r}')_{pq}$ is the element of the matrix of kinetic coefficients proportional to the inverse time of elementary diffusional jump of an oxygen atom from the site $(q,\mathbf{r}')$ to the site $(p,\mathbf{r})$; $\xi_p(\mathbf{r},t)$ is the random noise term. This term simulates fluctuations which allow a system to avoid trapping in free-energy local minima (metastable states). The variational derivative $\delta F/\delta n_q(\mathbf{r}',t)$ is the driving force of the transformation expressed through the interaction energies of oxygen ion pairs $W(\mathbf{r}-\mathbf{r}')_{pq}=W_i$. Equation (10) describes an atomic random walk of interacting oxygen atoms. In our simulation, the nearest-neighbor model for $L(\mathbf{r}-\mathbf{r}')_{pq}$ is assumed. The random noise function $\xi_p(\mathbf{r},t)$ satisfies the usual correlation condition

$$\langle\xi_p(\mathbf{r},t)\xi_q(\mathbf{r}',t')\rangle=2k_BTL_{pq}(\mathbf{r}-\mathbf{r}')\delta(t-t'),$$

where T is the absolute temperature. To simulate the noise meeting this condition, a random number generator is used. The computational procedure used in this work is exactly the same as in our previous study.[14] The details can be found in Refs. 14 and 19. As before, oxygen ordering is described by the Ising model so that all structural states are obtained by the oxygen atoms redistribution over interstitial sites of two oxygen occupation sublattices $(p,q=1,2)$ located in a basal Cu(1)-O(001) plane of $YBa_2Cu_3O_{6+x}$.

To get the explicit form of the kinetic equation, we have to specify the free-energy functional F. In the effective mean-field approximation used in this paper, the free energy F has the form

$$F=\frac{1}{2N}\sum_{\mathbf{pq}}\sum_{\mathbf{k}}V(\mathbf{k})_{pq}\tilde{n}_p(\mathbf{k})\tilde{n}_q(\mathbf{k})^*$$
$$-T\sum_{\mathbf{r}}\sum_{q=1}^{q=2}\{n_p(\mathbf{r})\ln n_p(\mathbf{r})+[1-n_p(\mathbf{r})]\ln[1-n_p(\mathbf{r})]\}, \tag{11}$$

where $\tilde{n}_p(\mathbf{k})$ is the Fourier transform of $n_p(\mathbf{r})$ and the summation in $\mathbf{k}$ is carried out over the first Brillouin zone of the O-I phase. Both F and the transformation driving force $\delta F/\delta n_q(\mathbf{r}',t)$ of the kinetic equation (10) are determined by the Fourier transforms $V(\mathbf{k})_{pq}$ of the O-O interaction energies $W(\mathbf{r})_{pq}=W_i$ which were calculated only once at a given x.

The simulation of the oxygen ordering kinetics is obtained by numerical solution of the kinetic equation (10) with the periodical boundary conditions. The computational cell consists of 60×60 (in some cases 120×120 and 70×70) unit cells in the Cu(1)-O(001) basal plane. Equation (10) is for-

mulated in a dimensionless form using the reduced time $t^*=t/\tau$ [where $\tau=(4AL_1)^{-1}$ is the typical time of an elementary diffusion event, $A=(z^*)^2\sqrt{2}/a_0$, a_0 is the perovskite lattice parameter, L_1 is the kinetic coefficient $L(\mathbf{r}-\mathbf{r}')_{pq}$ for the nearest-neighbor diffusional jump]. Equation (10) was solved with respect to the $2N$ values of $n_p(\mathbf{r},t)$ using a recurrence formula:

$$n_p(\mathbf{r},t^*+\Delta t^*)=n_p(\mathbf{r},t^*)+\Delta t^*\,\frac{dn_p(\mathbf{r},t^*)}{dt^*}, \qquad (12)$$

where $dn_p(\mathbf{r},t^*)/dt^*$ is expressed by the right-hand side of Eq. (10), and Δt^* is the reduced-time increment. Equation (12), actually, relates $n_p(\mathbf{r},t^*)$ and $n_p(\mathbf{r},t^*+\Delta t^*)$. The temporal dependence of $n_p(\mathbf{r},t^*)$ is obtained by applying Eq. (12) at consecutive moments of time. The time increment Δt^* was usually equal $\Delta t^*\sim10^{-3}$. The coordinate and temporal dependence of $n_p(\mathbf{r},t)$ describes the atomic and mesoscale structure evolution occurring along the transformation path.

In this study we performed computer simulation of the secondary and tertiary ordering which develops upon cooling the O-I primary ordered structure. Therefore, the temperatures used in the computer simulation were always below the temperature T_0 of the $T\rightarrow$O-I transition. The oxygen ordering kinetics was initiated by ''quenching'' (or a step-down cooling) a domain of the O-I phase to room temperature $T_{\rm room}$ (or to another temperature T_a) and subsequent ''annealing'' at this temperature.

V. COMPUTER SIMULATION RESULTS

A. Stable ordered phases at $x=3/5$, 2/3, and 3/4

In this section, we present some results of the computer simulation of ordering in $YBa_2Cu_3O_{6+x}$. The simulation was performed with the effective O-O pair-interaction energies consisting of two parts [Eqs. (3)], the anisotropic screened Coulomb energies $W(\mathbf{r}-\mathbf{r}')^f_{pq}$, given by Eq. (4) and the strain-induced energies $W(\mathbf{r}-\mathbf{r}')^{\rm elast}_{pq}$ whose Fourier transforms were calculated by using Eqs. (A1)–(A5). Parameters of the potential $W(\mathbf{r}-\mathbf{r}')^f_{pq}$ are presented in Fig. 2.

To get a rough idea about the choice of the simulated ''heat treatment'' regime, we, first, analyzed the relative stability of different ordered phases and determined the mutual location of their stability fields on the phase diagram. This was done by comparison of the equilibrium free energy F [Eq. (11)] of different ordered phases at a given x and T. To find the equilibrium free energy of an ordered phase, we numerically solved Eq. (10) with the function $n_p(\mathbf{r},t^*=0)$ describing the initial state ($t^*=0$) as a single-domain state of this phase at a given composition x. This initial state was then allowed to relax during the ordering kinetics at a given temperature T. The corresponding free energy decreases with time until it starts to oscillate around some average value at time $t^*=t^*_\infty$. This value corresponds to the free-energy minimum describing the equilibrium state. In many cases, the equilibrium state was reached only after a very long ''annealing'' time ($t^*_\infty\geqslant1000-2000$). The resultant function $n_p(\mathbf{r},t^*_\infty)$ for $t^*=t^*_\infty$ describes the equilibrium state corresponding to the free-energy minimum. The equilibrium free energy was calculated by substituting $n_p(\mathbf{r},t^*_\infty)$ to Eq. (11).

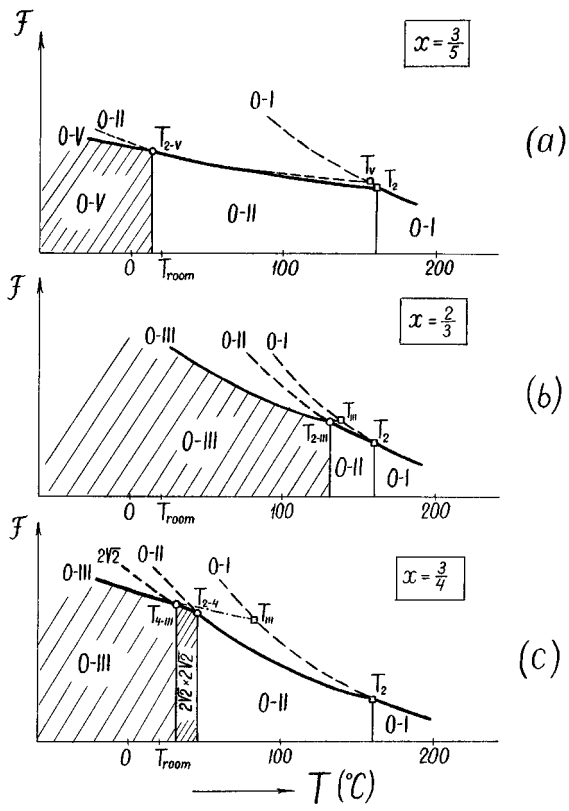

FIG. 3. The schematic temperature dependences of the free energies F for different ordered phases calculated from Eq. (11) for the stoichiometries, $x=3/5$ (a), $x=2/3$ (b), and $x=3/4$ (c). The temperature ranges of stability for different ordered phases are found by comparison of the minimum free energies of competing phases. The shaded area represents the temperature range of stability of the low-temperature stable phase. The squares represent the absolute instability temperatures T_-: the temperatures T_2 for the O-I→O-II and $T_{\rm III}$ for the O-I→O-III transitions [Eqs. (5a) and (5b)] and $T_{\rm V}$ for the O-I→O-V transition. The circles represent the first-order transition temperatures where the free energies of two phases are equal ($T_{2\text{-III}}$ for the O-II→O-III transition, $T_{2\text{-V}}$ for the O-II→O-V transition, $T_{2\text{-4}}$ and $T_{4\text{-III}}$ for the O-II→$2\sqrt{2}a_0\times2\sqrt{2}a_0$ and $2\sqrt{2}a_0\times2\sqrt{2}a_0$→O-III transitions, respectively). The O-II →O-III transition (b) is kinetically hindered and only the O-I→O-III transition develops if the O-I phase is quenched fast directly to the O-III phase field (into the shaded area). The O-II→O-V transition illustrated in (a) is also kinetically hindered.

This procedure was performed for the O-I, O-II, and O-III phases and also for the $(5a_0\times a_0)$ Magneli phase and the $2\sqrt{2}a_0\times2\sqrt{2}a_0$ phase, each at a given composition x. The results of comparison of the equilibrium free energies of these phases for the several stoichiometries $x=2/3$, 3/5, and 3/4 are presented in Fig. 3. Figure 3 gives only the schematic representation of the temperature dependence of the free energy since the difference in free energies of competing low-temperature phases is too small near the transition temperature ($\Delta F/F\sim10^{-5}-10^{-6}$) to be shown in the same scale for all competing phases considered at given x,T. However, these dependences $F(T)$ do give the correct mutual position of the stability fields of different phases and the correct temperature coordinates of intersection points corresponding to the transition temperatures.

A square in Fig. 3 represents the absolute instability temperature T, the temperature where the O-I phase becomes unstable with respect to the infinitesimal fluctuations of the long-range order (LRO) parameter of the corresponding secondary ordered phase. These are the temperature T_2 for O-I→O-II, T_{III} for O-I→O-III, and T_V for O-I→O-V transitions, respectively. The temperature T_V is determined by the equation

$$T_V = -2c(1-2c)V_{22}(\tfrac{2}{5}00),$$

which is similar to Eqs. (5a) and (5b). The circle represents the first-order transition temperature where the free energies of two phases become equal to each other. The first-order transition temperatures are designated $T_{2\text{-III}}$ for the O-II →O-III transition, $T_{2\text{-V}}$ for the O-II→O-V transition, $T_{2\text{-4}}$ and $T_{4\text{-III}}$ for the O-II→$2\sqrt{2}a_0\times 2\sqrt{2}a_0$ and $2\sqrt{2}a_0\times 2\sqrt{2}a_0$ →O- III transitions, respectively. Shaded areas at low temperatures represent the stability fields of the low-temperature phases.

It follows from Fig. 3(a) that our O-O potential provides the thermodynamic stability of the O-V phase (which is the $5a_0\times a_0$ or the [(2/5)00] Magneli phase) near the room temperature T_{room} ($T_{2\text{-V}}\sim 13\ ^\circ\mathrm{C}\sim T_{\mathrm{room}}$) and the stoichiometric composition of this phase $x=3/5$. The computer-simulated microstructure showing small microdomains of this Magneli phase (at the ''annealing'' temperature $T=0\ ^\circ\mathrm{C}<T_{2\text{-V}}$) is presented in Fig. 4 and will be discussed later.

Figure 3(b) shows that the O-III phase has a wide temperature range of stability at its stoichiometric composition $x=2/3$, spreading below the transition temperature $T_{2\text{-III}}\sim 133\ ^\circ\mathrm{C}$ which is very close to the estimated temperature of the O-I→O-III transition, $T_{\mathrm{III}}\sim 136\ ^\circ\mathrm{C}$. Both temperatures, T_{III} and $T_{2\text{-III}}$, are higher than the annealing temperature $T=120\ ^\circ\mathrm{C}$, used in Ref. 16 to obtain the O-III phase (this temperature $T=120\ ^\circ\mathrm{C}$ is within the stability field of the O-III phase).

Although the O-II→O-III transition is thermodynamically possible, our computer simulation and analysis presented in the Discussion show that this transition is kinetically hindered. The O-III phase can be formed only in the first-order O-I→O-III transition which can be realized if the O-I phase is directly ''quenched'' into the O-III phase field (shaded area) below $T_{2\text{-III}}\sim 133\ ^\circ\mathrm{C}$.

The same conclusions are true for the O-I→O-V and O-II→O-V transitions at $x=3/5$ [Fig. 3(a)]. It could be shown that the kinetics of the O-II→O-V ordering is similar to that of the O-II→O-III ordering and that it could be easier to obtain the O-V phase by ''quenching'' the O-I phase directly to the O-V field.

Figure 3(c) shows that the O-O potential found in this work provides a very narrow temperature range of stability of the $2\sqrt{2}a_0\times 2\sqrt{2}a_0$ phase at $x=3/4$. It is located between the temperatures $T_{4\text{-III}}\sim 32\ ^\circ\mathrm{C}$ and $T_{2\text{-4}}\sim 45\ ^\circ\mathrm{C}$. At lower temperatures, $T<T_{4\text{-III}}$, the O-III phase becomes more stable than the $2\sqrt{2}a_0\times 2\sqrt{2}a_0$ phase. This is in agreement with the x-ray study where the O-III phase rather than $2\sqrt{2}a_0\times 2\sqrt{2}a_0$ phase was found in quenched samples with stoichiometries $x\sim 0.7\pm 0.03$ and $x\sim 0.75\pm 0.03$.[23]

The results of the thermodynamic analysis presented in Fig. 3(c) indicate that the O-III phase is stable not only at its exact stoichiometry $x=2/3$ [Fig. 3(b)], but also at $x>2/3$. However, the $2\sqrt{2}a_0\times 2\sqrt{2}a_0$ phase may form near $x\sim 3/4$, its exact stoichiometry. Results of computer simulations for $x\sim 3/4$ will be described later.

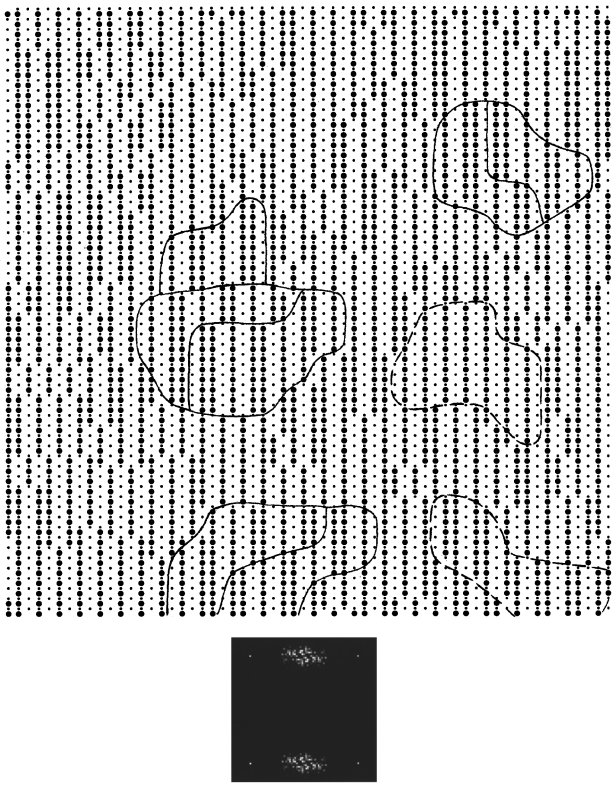

FIG. 4. Simulated microstructure and its diffraction pattern obtained by ''quenching'' a nonstoichiometric ($x=3/5$) domain of the O-I phase to the temperature $T\sim 0\ ^\circ\mathrm{C}$ and the following ''annealing'' at $T\sim 0\ ^\circ\mathrm{C}$ during the time $t^*=1440$. The obtained microstructure is not the equilibrium O-V (or $5a_0\times a_0$) Magneli phase but a frozen metastable state which does not change with increase of the annealing time (at $t^*>500$). It consists of a mixture of small domains of O-V, O-II and O-III phases. Several domains of O-V are encircled by solid lines. Some of domains of the O-II and O-III phases are shown by a dashed line. Oxygen atoms (large circles) are shown in the interstitial positions if the occupation probability $n_p(\mathbf{r},t^*)>x=3/5$, small solid circles are the Cu atoms. The bottom part presents the corresponding intensity distribution within a unit cell of the reciprocal lattice of the O-I phase, four sharp points are the fundamental points (00), (10), (01), and (11) in the (001) plane. The mixture of small domains of different order produces diffuse-type streaks in the [100] direction [perpendicular to the Cu(1)-O chains] which are centered at the [(1/2)00]-type points. The model crystal consists of 60×60 unit cells.

B. Simulated microstructures

Figures 4–7 present several results of computer simulations for the representative stoichiometries $x=3/5$, $x=2/3$, and $x=3/4$, which are the most interesting for comparing the simulated microstructures and diffraction patterns with observation results. On simulated microstructures given in Figs. 4–7, the oxygen atoms are shown by large circles if the occupation probability $n_p(\mathbf{r},t^*)>x$, small solid circles are the Cu(1) atoms.

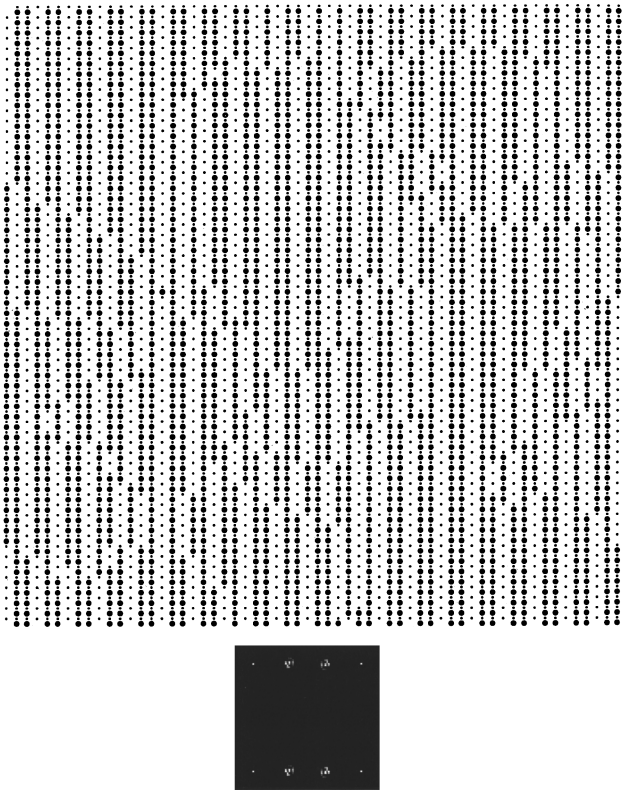

FIG. 5. Simulated microstructure and its diffraction pattern obtained by ''quenching'' of a nonstoichiometric ($x=2/3$) domain of the O-I phase to the temperature T_{room} and ''annealing'' at T_{room} during the time $t^*=1920$. The temperature T_{room} is within the stability field of the O-III phase [Fig. 3(b)]. The microstructure presents a practically pure O-III phase. Oxygen atoms (large circles) are shown in the interstitial positions if the occupation probabilities $n_p(\mathbf{r},t^*)>x=2/3$, small solid circles are the Cu atoms. The bottom part presents the corresponding intensity distribution within a unit cell of the reciprocal lattice of the O-I phase, the four sharp points are the fundamental points (00), (10), (01), and (11) in the (001) plane. Strong diffuse maxima centered at [(1/3)00] and [(2/3)00] types are the superlattice points of the O-III phase. This diffraction pattern is in agreement with the observation (Ref. 16) after the analogous heat treatment quenching of the O-I phase ($T_{\text{quen}}=259$ °C) to T_{room}. The model crystal consists of 60×60 unit cells.

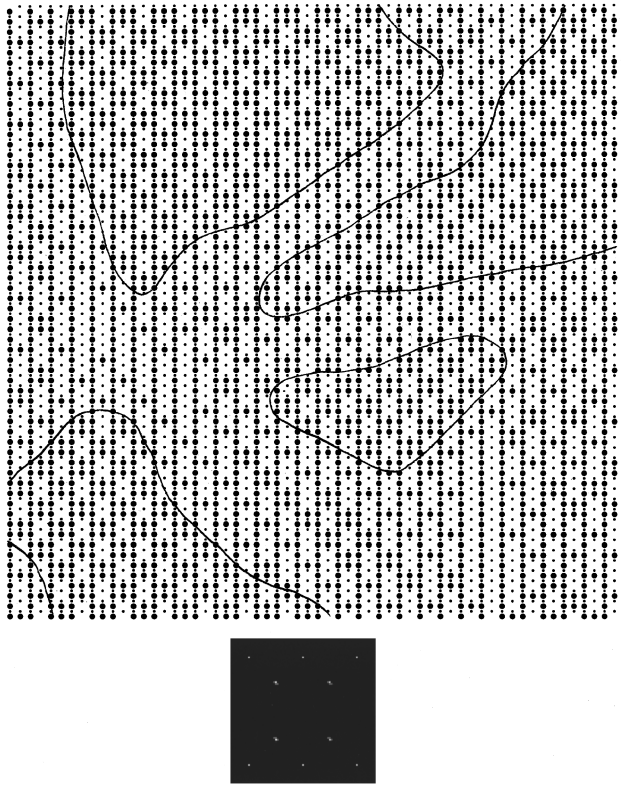

FIG. 6. Simulated microstructure and its diffraction pattern obtained by ''quenching'' a nonstoichiometric ($x=3/4$) domain of the secondary ordered O-II phase to the temperature T_{room} and ''annealing'' at T_{room} during the time $t^*=960$. The microstructure consists of large domains of the $2\sqrt{2}a_0\times 2\sqrt{2}a_0$ phase formed in the tertiary ordering O-II$\rightarrow 2\sqrt{2}a_0\times 2\sqrt{2}a_0$ and the remaining pieces of an intermediate structure. Oxygen atoms (large circles) are shown in the interstitial positions if the occupation probabilities $n_p(\mathbf{r},t^*)>x=3/4$, small solid circles are the Cu atoms. The bottom part presents the corresponding intensity distribution within a reciprocal unit cell of the O-I lattice, four sharp points near the borders are the fundamental points (00), (10), (01), and (11) in the (001) plane. Diffraction presents two {(1/2)00}-type maxima of the parent O-II phase and four sharp and strong {(1/4)(1/4)0}-type maxima of the tertiary ordered $2\sqrt{2}a_0\times 2\sqrt{2}a_0$ phase (located in the middle of the pattern), their intensity increasing with the annealing time. The model crystal consists of 60×60 unit cells.

It should be borne in mind that the system may be caught at local free-energy minima (shallow metastable states) during the diffusional relaxation process. Its escape from the minima can occur only by the fluctuation mechanism, viz. by thermal nucleation of a more stable structural state. To shorten a waiting time for such a nucleation, the increased values of the random fluctuations $\xi_p(\mathbf{r},t^*)$ [Eq. (10)] were used (these values, however, were small enough to guarantee the free-energy relaxation). When the free energy ceases to decrease and starts to oscillate around a certain average value, the noise $\xi_p(r,t^*)$ is decreased to permit further free-energy reduction and eventually is reduced to zero to allow the system to reach the lower free-energy state.

To study the secondary ordering within the nonstoichiometric O-I phase, we simulated the ordering kinetics by choosing a single-domain or a microtwinned state of O-I phase as the initial state. To simulate the tertiary ordering, we chose the nonstoichiometric O-II phase state as the initial state.

1. Stoichiometry x =3/5

Since the diffraction pattern of the O-V Magneli phase, characterized by the diffuse maxima at {(2/5)00} and {(3/5)00} points, was observed in several studies,[7,25,26] it was interesting to study the ordering at the exact stoichiometry of this phase, $x=3/5$. As follows from Fig. 3(a), the O-V phase is stable at temperatures below the transition temperature $T_{2-\text{V}}\sim 13$ °C. The results of the computer simulation of the O-V phase ordering are shown in Fig. 4. A nonstoichiometric domain of the O-I phase ($x=3/5$) is ''quenched'' to the temperature $T\sim 0$ °C$<T_{2-\text{V}}$, i.e., inside the stability field of the O-V phase, and then ''annealed'' during the time $t^*=1440$

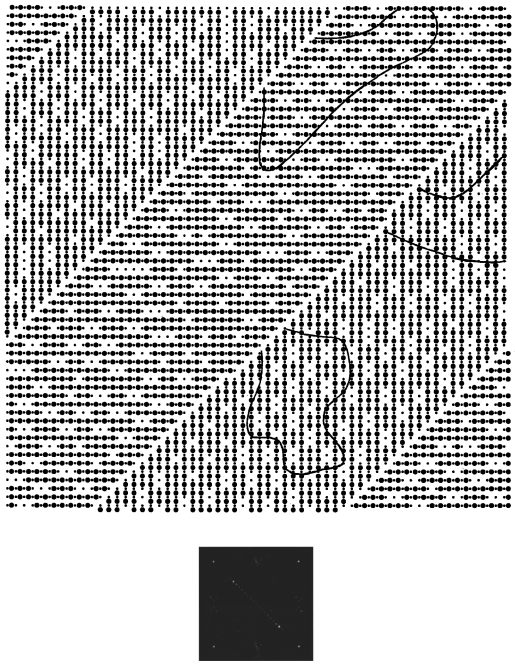

FIG. 7. Simulated microstructure and the corresponding diffraction pattern obtained by two-step ''quenching'' of the (110) twins of the nonstoichiometric ($x=3/4$) O-I phase ($t^*=240$ at $T=41$ °C and $t^*=720$ at $T=T_{\text{room}}$). The (110) twin boundary is the nucleation site facilitating the formation of the $2\sqrt{2}a_0\times 2\sqrt{2}a_0$ phase. Several small domains of the $2\sqrt{2}a_0\times 2\sqrt{2}a_0$ phase of two orientation variants formed within O-I twins are encircled. Oxygen atoms (large circles) are shown in the interstitial positions if the occupation probabilities $n_p(\mathbf{r},t^*)>x/2=0.375$, small solid circles are the Cu atoms. The bottom part presents the corresponding intensity distribution within the reciprocal unit cell of the O-I lattice, the four sharp points near the borders are the fundamental points (00), (10), (01), and (11) in the (001) plane. The diffraction pattern reveals two diffraction spots (which are as strong and sharp as those in Fig. 6) in $\pm[(1/4)(1/4)0]$ positions, located on the [110] direction perpendicular to the (110) twin planes. Hardly visible traces of extremely wide {(1/2)00}-type maxima of the O-II phase can be noticed. The streak in the [110] direction across the {(1/4)(1/4)0}-type maxima is a result of diffraction from the periodical array of the (110) twin-related domains associated with the periodical boundary conditions. The model crystal consists of 60×60 unit cells.

at $T\sim 0$ °C. Figure 4 shows that simulated ordering produces a mixture of small ordered domains of different types. It is easy to detect the domains of three phases: O-V, O-II, and O-III. The domains of the O-V phase are encircled by the solid line. Some of domains of the O-II and O-III phases are shown by the dashed line. Although the O-V phase is a stable phase at the temperature of the computer simulation, $T\sim 0$ °C, its equilibrium single-phase state is not reached. Computer simulation of the kinetics process indicates that after a certain time, $t^*\sim 500$, the system freezes in a metastable state along the transformation paths, the microstructure and the diffraction pattern actually do not change with a further ''annealing'' at $t^*>500$. We note that domains of the O-V phase are formed only in the O-I→O-V reaction and not in the O-II→O-V reaction.

The bottom part of Fig. 4 shows the diffraction pattern calculated for the simulated microstructure presented at the top of this figure. The intensity is assumed to be proportional to the squared Fourier transform, $I(\mathbf{k})\sim|\tilde{n}_2(\mathbf{k})|^2$, of the occupation probabilities $n_2(\mathbf{r})$. The diffuse scattering pattern is visualized by shadows of gray which are determined by the value of $I(\mathbf{k})$. The larger is the value of $I(\mathbf{k})$, the lighter the color. Figure 4 shows the diffuse scattering maxima having a shape of a streak centered at the [(1/2)00] point which is perpendicular to the Cu(1)-O chains. The same type of diffuse scattering was reported in many studies. Four sharp points, on the corners of the reciprocal unit cell in the (001) plane (they present in Figs. 4–7), correspond to the fundamental diffraction maxima of the O-I phase, (00), (10), (01), and (11).

2. Stoichiometry x =2/3

As noted in Sec. II B (see also the Discussion), the O-III phase is expected to form easily from the O-I phase, if the latter is quenched directly into the stability field of the O-III phase (below $T_{2-\text{III}}\sim T_{\text{III}}\sim 130$ °C), but its formation from the O-II phase is kinetically hindered. The observations in Ref. 16 seem to agree with this expectation. A lack of the O-II→O-III transition is an important conclusion which, if it is proved to be correct, would give a clue for the suggestion of the heat treatment regime producing the O-III phase. It is interesting to check whether the computer simulation of ordering at $x\sim 2/3$ confirms this conclusion.

We simulated both heat treatment regimes used in Ref. 16 to obtain the O-III phase. First, we simulated the 120 °C annealing by brining a single-domain state of the O-I phase at $x=2/3$ to $T=120$ ° and by ''annealing'' it at this temperature during time $t^*=960$. After that, the system was steplike ''cooled'' to T_{room} during $t^*=480$ and finally ''annealed'' at T_{room} during time $t^*=1920$ until the evolution of the intensity of the [(1/3)00] maxima practically stopped. This ''heat treatment'' produced large domains of the practically pure O-III phase which is in agreement with the observations.[16]

The other heat treatment used in Ref. 16 was also mimicked. We ''quenched'' a single-domain state of the O-I phase to $T=T_{\text{room}}$ and ''annealed'' it at T_{room} during time $t^*=1920$. The simulated microstructure is presented in Fig. 5. It shows domains of different sizes of the nearly pure O-III phase. The diffuse scattering calculated for this structure is shown on the bottom of Fig. 5 where sufficiently strong diffuse maxima centered at [(1/3)00] and [(2/3)00] superlattice points of the O-III phase can be clearly seen. This result is also in agreement with the observation.[16]

Finally, if the system is cooled slowly, it spends a comparatively long time within the O-II phase stability field before it eventually reaches the O-III phase stability field. If the cooling rate is low enough, the time spent within the O-II field is sufficiently long to accomplish the O-I→O-II transition. If this is the case, the cooling eventually brings the domains of the O-II phase into the O-III phase stability field. According to the thermodynamics, annealing of the O-II phase within the stability field of the O-III phase would result in the O-II→O-III transition. The question whether this transition really occurs within the stability range of the O-III phase is checked in our computer simulation. To do this, a nonstoichiometric ($x=2/3$) single domain of the O-II phase was ''annealed'' at $T=T_{\text{room}}$. It was shown that, irrespective of the annealing time and amplitudes of fluctuations, the O-II

phase does not transform to the O-III phase. This result supports the conclusion that the slow cooling regime just gives the O-II order and does not favor formation of the O-III phase.

3. Stoichiometry x=3/4

It was noted above that our ordering model predicts the stable $2\sqrt{2}\ a_0\times 2\sqrt{2}a_0$ phase at $x=3/4$ within a very narrow temperature interval above $T_{\rm room}$ [see Fig. 3(c)]. Since the thermodynamic analysis results in the O-II$\rightleftharpoons 2\sqrt{2}a_0\times 2\sqrt{2}a_0$ transition line T_{2-4} on the phase diagram, a natural way to investigate this ordering is to undercool a nonstoichiometric domain of the O-II phase ($x=3/4$) to the temperature T below $T_{2-4}\sim 45$ °C. The simulated structure obtained by this ordering at $T=T_{\rm room}$ is illustrated by Fig. 6. The structure consists of large domains of the $2\sqrt{2}a_0\times 2\sqrt{2}a_0$ phase and residual fragments of an intermediate structure. The corresponding diffraction pattern, on the bottom part of Fig. 6, besides two maxima of the {(1/2)0 0} type also has four sharp and strong maxima of {(1/4)(1/4)0} type (located in the central part of the diffraction pattern presenting the reciprocal unit cell) whose intensity gradually increases with the annealing time.

To investigate different ''heat treatments'' that may result in formation of the $2\sqrt{2}\ a_0\times 2\sqrt{2}a_0$ phase, we also explored the possibility of the direct O-I$\rightarrow 2\sqrt{2}\ a_0\times 2\sqrt{2}a_0$ ordering. To do this, we performed the computer ''experiment'' under two other conditions. We simulated ordering (i) in a domain of the O-I phase and (ii) in two (110)-twin related domains of the O-I phase. ''Quenching'' or ''cooling'' to $T_{\rm room}$ of a O-I phase domain [case (i)] produced the diffraction pattern with weak and broad diffuse maxima near {(1/4)(1/4)0} points, which were noticeably shifted from the exact {(1/4)(1/4)0} positions.

However, ''quenching'' to $T_{\rm room}$ of the twinned O-I phase [case (ii)] gives a different result shown in Fig. 7. In this case, ordering inside the components of the (110) twin produces two twin-related orientation variants of the $2\sqrt{2}\ a_0\times 2\sqrt{2}a_0$ phase. They generate two diffraction maxima corresponding to the generic reciprocal-lattice vectors $\pm$[(1/4)(1/4)0] perpendicular to these twins. Figure 7 shows that these maxima are as strong and sharp as those obtained by ordering within a domain of the O-II phase (Fig. 6).

The ordering inside the (110) twins also produces two twin-related orientation variants of the $2\sqrt{2}\ a_0\times 2\sqrt{2}a_0$ phase but with the (110) boundary. They also generate two diffraction maxima, but at the $\pm$[(1/4)(1/4)0] points. Since a real material usually has both systems of the O-I phase twins, they should produce the diffraction pattern having the whole family of four {(1/4)(1/4)0}-type maxima. We note that the diffraction pattern also has {1/200}-type diffuse maxima but they are by an order of magnitude weaker and wider to compare with the strong and sharp {(1/4)(1/4)0}-type maxima (compare Figs. 6 and 7). A special role played by the {110} twins of the O-I phase in formation of the $2\sqrt{2}\ a_0\times 2\sqrt{2}a_0$ phase at $x\sim 3/4$ is addressed in the Discussion.

VI. DISCUSSION

According to the third law of the thermodynamics, cooling a nonstoichiometric ordered system always results in increase of the long-range order. In a conventional nonstoichiometric system, this increase occurs by decomposition into a mixture of ordered phases (or ordered and disordered phases) whose stoichiometries are closer to the ideal ones. However, this is not the case with the $YBa_2Cu_3O_{6+x}$ oxides. The decomposition in $YBa_2Cu_3O_{6+x}$, which could bring the stoichiometries of the ordered phases closer to their ideal stoichiometries, is suppressed. These ideal stoichiometries $x_{\rm st}$ are 1/2 for the O-II phase, 2/3 for the O-III phase, 3/5 for the O-V phase, and 3/4 for the $2\sqrt{2}\ a_0\times 2\sqrt{2}a_0$ phase. The nonstoichiometric $YBa_2Cu_3O_{6+x}$ oxide reaches its ideal stoichiometry by a sequence of congruent multiple ordering (primary, secondary, tertiary, etc.) maintaining an initial spatially homogeneous composition x. Each new ordered phase in this sequence has the ideal stoichiometry which is closer to its real composition x than the previous ordered phase formed at a higher temperature. An example of such a sequence of ordering reactions is the sequence $T\rightarrow$O-I $\rightarrow$O-II$\rightarrow 2\sqrt{2}\ a_0\times 2\sqrt{2}a_0$ phases developing upon cooling the system with the stoichiometry $x=3/4$. This congruent ordering mechanism of stoichiometry accommodation is the main reason for formation of a variety of ordered states observed in $YBa_2Cu_3O_{6+x}$.

The theoretical modeling of the specific ordering behavior in this system requires development of the oxygen ordering model which would be able to reproduce the well-known characteristics of ordering in $YBa_2Cu_3O_{6+x}$ and to predict its unknown features. It should provide the ordering temperatures which are close to the recent experimental data[15,16] for the O-II and O-III phases as well as to provide a good agreement between the calculated and measured shape of the {(1/2)00}-type diffuse maxima on the diffraction pattern of the O-II ordered phase.[15,17]

Our computer simulation demonstrates that ''cooling'' of $YBa_2Cu_3O_{6+x}$ really does not produce the decomposition. Instead, the system undergoes the multiple ordering which turns out to be a mode of stoichiometry accommodation. This unusual behavior is associated with the long-range and repulsive character of the adopted O-O interaction potential. With this potential, an aggregation of the repelling O atoms into islands of oxygen-rich phase during decomposition would result in a significant free energy increase and thus would suppress the decomposition. The strain-induced O-O interaction, which was taken into consideration, also plays an important role. Although its contribution to the total O-O interaction energy is quite small [only $\sim$5% for the Fourier component V_{22}[(1/2)00] and even less for the eigenvalue $\lambda(000)_-$], it is responsible for formation of the strain-accommodating mesoscopic tweed and polytwin morphologies which are observed at $x>0.5$.

The computer simulation based on our model is able to predict the appearance of the O-III and O-V Magneli phases at room temperature at which these phases were detected in Refs. 4, 16, 23, 25, and 26 (our previous more crude model was not able to do so). What is even more interesting, the computer simulation allows us to explain the specific kinetic features which prevent the O-II$\rightarrow$O-III and O-II$\rightarrow$O-V tertiary ordering and to make predictions on possible kinetic regimes which could facilitate formation of the O-III, O-V, and $2\sqrt{2}a_0\times 2\sqrt{2}a_0$ phases.

A very interesting fact is that the ordering model formu-

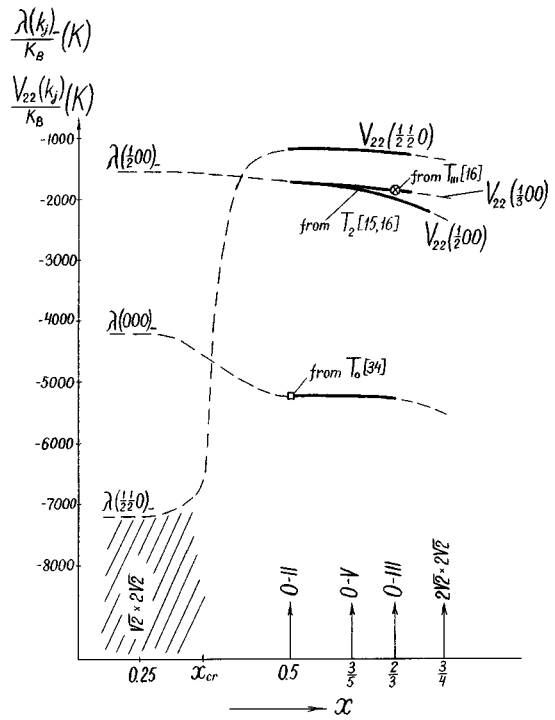

FIG. 8. Dependences of $V_{22}(\mathbf{k}_i)$ and the eigenvalues $\lambda(\mathbf{k}_i)_-$ of the O-O interaction potential estimated from experimental data (Refs. 15–17 and 34). The curve V_{22} [(1/2)00] at $0.5<x\leqslant 0.7$ is estimated from the observed temperature T_2 of the O-I→O-II transition [Eq. (5a), the solid line in Fig. 1] (Refs. 15 and 16), the value V_{22}[(1/3)00] at $x\sim 2/3$, from the estimated transition temperature T_{III} [Eq. (8a), the encircled cross in Fig. 1] (Ref. 16). The value $\lambda(000)_-/k_B\sim -5190$ K at $x=0.5$ is estimated from the observed temperature $T_0\sim 700$ °C of the T→O-I transition (Ref. 34). The eigenvalues $\lambda(000)_-$, $\lambda[(1/2)00]_-$, and $\lambda[(1/2)(1/2)0]_-$ at $x\sim 0.25$ and 0.5 were found in Ref. 14. Arrows along the x axis indicate the stoichiometries of the observed superstructures. Dashed-line segments at $x>2/3$ are the extended parts of the corresponding dependences which are not covered by experimental data (Refs. 15–17).

lated in this paper on the basis of recent experimental data shows an interesting correlation between the O-O bonds responsible for oxygen ordering and the high-temperature superconductivity. As follows from the concentration wave theory of ordering[28,29] and particularly from Eq. (5), each type of ordering is determined by the special combination of the O-O interaction energies given by the Fourier transforms $V_{22}(\mathbf{k}_j)$ of the O-O interaction energies and their eigenvalues $\lambda(\mathbf{k}_j)_-$ at the positions of the main superlattice points $\mathbf{k}_j$. Figure 8 illustrates the concentration dependence of some $V_{22}(\mathbf{k}_j)$ and $\lambda(\mathbf{k}_j)_-$, corresponding to the observed ordered states in this system, which were obtained by fitting to the observed ordering temperatures. Figure 8 puts together the data obtained earlier at $x<0.4$ (Ref. 14) and those obtained in this study for $x>0.4$–0.5. It shows that the Fourier transform $V_{22}[(1/2)(1/2)0]=\lambda[(1/2)(1/2)0]_-$ of the O-O potential undergoes a drastic change around $x=x_{\mathrm{cr}}\sim 0.35$. By the way, it is this change that is actually responsible for different character of ordering on both sides of x_{cr} which results in the [110] chain-ordered structures at $x<x_{\mathrm{cr}}\sim 0.35$ and the [010] chain-ordered structures at $x>\sim 0.35$. In terms of the individual effective O-O pair energies $W(\mathbf{r}-\mathbf{r}')_{\mathrm{pq}}=\mathrm{W_i}$, the drastic change in $V_{22}[(1/2)(1/2)0]$ shown in Fig. 8 is mostly associated with the change in the covalent bonding energy of the next-nearest O-O pairs [the values $\delta W_2(x)$ and $f(x)$ in Fig. 2, see Eq. (4)].

This effect is fully in line with the sharp changes of other physical properties observed in this system (change in bond lengths, valence sums, lattice parameters, etc.) occurring around x_{cr}.[4,36] However, the most interesting fact is that the sharp change in the oxygen bond energies at $x\sim 0.35$ (Fig. 8) occurs near the same composition $x_{\mathrm{cr}}\sim 0.35$ where the transition from the semiconducting to the high-temperature superconducting state is observed. Therefore, the high-temperature superconductivity in this system is closely correlated with the oxygen-oxygen interaction, which, in turn, determines the character of oxygen ordering. The correlation in behavior of all above-mentioned physical properties seems to be caused by the same underlying effect, the drastic reconstruction of the electronic spectrum near the threshold value x_{cr}.

Stable ordered phases

The ordering model proposed in this paper allowed us to investigate the structural transformations in $YBa_2Cu_3O_{6+x}$ and find the structural states along the ordering path. These structural states are not necessarily the stable states corresponding to the true equilibrium and thus their existence can not always be obtained from the thermodynamic consideration alone. These states may be either kinetically frozen or metastable. However, in both cases, they are stable in the practical sense because they do not evolve during the physically long observation time; in fact, they are the structures that are really observed. Therefore, the computer simulation of the ordering kinetics is the most appropriate way for studying the structures of ordered phases of $YBa_2Cu_3O_{6+x}$. Figures 4–7 present several examples of the simulated microstructures and diffraction patterns (an example of the frozen state, for $x=3/5$, is given in Fig. 4) which reproduce the major observation results and allow us to elucidate some problems which are still under discussion.

The proposed ordering model also allowed us to compare the relative thermodynamic stability of different ordered phases and, particularly, to estimate the location of the stability fields of these phases on the phase diagram. Some of these results obtained at several important stoichiometries are illustrated by Fig. 3. The stability analysis was done by comparing the free energies (11) of these phases which were calculated by using the solution of the kinetic equation after ''equilibrating'' a single-domain state of each phase at given stoichiometry x and temperature T. This analysis gives important information because the atomic structures of microdomains appearing as a result of ordering of the disordered state can be compared with the atomic structure of the most stable phase predicted by the thermodynamics at given x and T. If these structures are different, this is an indication that the phase obtained in ordering is not stable and its appearance is associated with the specific character of the ordering kinetics.

It should be emphasized that all observed ordered phases, including the phases of different natures as the Magneli-type phases and $2\sqrt{2}a_0\times 2\sqrt{2}a_0$ phases, are obtained within the

same ordering model proposed in this paper. The previous models were not able to do so.[18–20,22]

1. O-II phase

Our computer simulations of the O-I→O-II ordering at x around $x=0.5$ reproduce several features that were observed for the O-II phase: (i) the O-II phase forms a system of ordered microdomains which do not grow unless the stoichiometry is practically equal to the exact stoichiometry of the O-II phase, $x=0.5$, (ii) the domains have anisotropic shape, which results in anisotropy of weak [(1/2)00]-type diffuse maxima. This is consistent with the observation results. Because of the weak diffuse maxima at the [(1/2)00] superlattice points, most researchers regard the O-II ordered state as a short-range order state even for the stoichiometric composition $x=0.5$ (for instance, Refs. 15 and 16).

Although the computer simulation gives the correct domain shape anisotropy, it, unfortunately, does not produce the observed domain sizes which are about $\sim 170\times 70$ Å at $x=0.50(5)$.[15] However, the latter is associated with the limited size of our computational cells, 60×60 and 120×120, rather than with shortcomings of our model.

The simulated annealing of $YBa_2Cu_3O_{6+x}$ within the O-II phase stability field produces the O-I→O-II ordering also at larger stoichiometries, close to $x\sim 2/3$. However, the [(1/2)00]-type diffuse maxima are even weaker at these x because of a smaller degree of the O-II-type order. This is in agreement with the observations where the [(1/2)00] diffuse maxima generated by the O-II phase were found at $x<\sim 0.65$–0.66, but were unnoticeable at larger x.[4,15,23,26]

2. O-III phase

Although the O-III phase was observed in several studies,[7,16,23,25,26] there is very little known about the mechanism of its formation. This phase may be formed upon cooling either by O-I→O-III secondary ordering or by O-II→O-III tertiary ordering. In both cases this ordering is the first-order transition requiring the nucleation. Qualitative arguments given below, together with a thorough analysis of all experimental data on both O-II and O-III phases and our computer-simulations results, allowed us to clarify the mechanism of formation of the O-III phase and to explain why it is so difficult to observe this phase. As a result, we are able to suggest the heat treatment regimes which would provide the O-III phase formation (see Secs. II B and III B).

It is shown in this study that the temperature range of stability of the O-III phase is located below the stability range of the O-II phase and thus the stability fields of both phases are separated by the O-II→O-III equilibrium line in the phase diagram [Fig. 3(b)]. Although the O-II→O-III ordering is thermodynamically feasible, it is kinetically hindered because the O-III phase symmetry is not a subgroup of the O-II phase symmetry. In this case, the O-III phase formation requires a drastic rearrangement of the atomic structure of the O-II parent phase, viz, disassembling the O-II phase atomic arrangement followed by reassembling it into the O-III phase atomic structure. This, however, is not the case for the O-I→O-III phase transition which is expected if the O-I phase is brought directly into the O-III phase field by quenching. The O-I→O-III ordering kinetics is not hindered since the O-III phase symmetry is a subgroup of the O-I phase symmetry and thus the O-III phase formation does not require the disassembling of the O-I phase atomic structure. Besides, the driving force of the O-I→O-III transition is also higher than that of the O-II→O-III transition because in the former case the high-temperature O-I phase is more strongly undercooled. Given all these factors, the O-I→O-III ordering develops much faster than the O-II→O-III transition. The latter would be a very slow process which would be hardly expected in the system. Contrary to that, the O-I→O-III ordering could be achieved if the O-I phase is quenched directly into the O-III phase stability field [$T<T_{\mathrm{III}}$, Fig. 3(b)] and this quenching is so fast that the competing O-I→O-II transition does not have enough time to develop during cooling across the O-II phase field. But after the O-I phase is brought into the O-III field, the O-III phase forms by annealing a sample within this field.

Therefore, to get a single-phase O-III ordered state, the O-I phase should be, first, annealed within the O-I phase stability field (at the temperature above the transition temperature $T_2=150$ °C–170 °C), this gives a good O-I-type order—and then sharply quenched (with the following annealing) to the O-III phase stability field [i.e., to the temperature below $T_{2\text{-III}}\approx 130$ °C, see Fig. 3(b)]. Samples where the O-III phase was observed were treated by a similar way: they were quenched from high temperatures rather than being slowly cooled.[16,23] Our computer simulation (see Sec. V B) confirms the above qualitative arguments. It shows that the O-III phase cannot be formed in the O-II→O-III transition but it easily forms in the O-I→O-III transition. Simulation results illustrating the O-I→O-III ordering transition in a quenched O-I domain are presented in Fig. 5.

3. Magneli-type phases

There are several features common for all Magneli-type phases that should be mentioned. All these phases have an $na_0\times a_0$ unit cell where n is the number of the phase in the series. The nth member of the series is formed by periodically faulting the atomic structure of the parent double-period O-II phase, viz. by the periodical insertion of an extra (100) oxygen plane into the O-II phase lattice, with a period equal to na_0.[1] The fault density is determined by deviation of the stoichiometry from $x=1/2$ (the higher the deviation, the greater the density) whereas its periodicity is established due to the repulsion of faults caused by repulsion of extra O atoms forming the fault planes. The higher the number n is, the greater the distance between the interacting faults is and thus the weaker this interaction is.

The computer simulations based on our model of oxygen ordering results in formation of the Magneli-type order. One of the requirements to the ordering model, which was used in this paper, is that the simulated ordering kinetics based on this model should reproduce the anisotropic shape of the diffuse maxima around the [(1/2)00] generic points. It turned out that the O-O interaction potential meeting this specific requirement leads to formation of the Magneli-type phases generating the [(1/3)00]-,{(2/5)00}-,[(3/7)00]-type diffuse maxima on the diffraction patterns.

Our estimates of the temperature stability range of the $5a_0\times a_0$ ordered phase (the O-V Magneli-type phase generating the [(2/5)00]-type diffuse maxima) near its exact sto-

ichiometry $x=3/5$ give this stability range at $T<T_{2-V}\sim 13$ °C [Fig. 3(a)]. [For the $7a_0\times a_0$ ordered phase, the found O-O interaction potential gives the transition temperature $T_{2-7}\sim 250$ (K) (at $x=4/7$), i.e., T_{2-7} is slightly below T_{room}].

The kinetics of ordering producing the O-V phase deserves a special discussion. Using the same line of reasoning as that for the O-III phase, it could be concluded that the O-II→O-V ordering is even more kinetically hindered than the O-II→O-III ordering (reassembling the $2a_0\times a_0$ atomic lattice into the $5a_0\times a_0$ lattice of the O-V phase is more difficult than reassembling the $2a_0\times a_0$ lattice into the $3a_0\times a_0$ lattice of the O-III phase) and that the O-V phase may be more easily obtained in the O-I→O-V transition. Besides, there is also another reason why formation of the O-V phase would be even more difficult than formation of the O-III phase: at $x=3/5$, the exact stoichiometry of the O-V phase, the O-II phase is less avoidable during the quenching. [The O-II phase is more stable, has a wider temperature stability range (down to $\sim T_{\text{room}}$), and a higher degree of order at $x=3/5$ than at $x\sim 2/3$.] The computer simulation performed at $x=3/5$ confirmed this conclusion: it showed that the O-V phase does not form in the O-II→O-V transition (by ''quenching'' a domain of the O-II phase into the O-V phase stability field) but it forms in the O-I→O-V transition (by ''quenching'' the domain of the O-I phase directly to the O-V phase stability field, i.e., to the temperature $T\sim 0$ °C$<T_{2-V}$, see Fig. 4). However, in the latter case, the ordering kinetics stops after a while and the system turns out to be frozen in a highly faulted mixture of very fine microdomains of the O-V phase (pieces consisting of $\sim 8\times 3$ unit cells are outlined in Fig. 4). This faulted microstructure could also be interpreted in terms of very small ordered domains of the O-II and O-III phases imbedded into the O-V microdomain structure. Actually, the appearance of a mixture of all three types of order, O-V, O-III, and O-II, is a result of the small difference between the free energies of all these phases.

The selected area electron-diffraction data[25] seem to agree with the simulation results. The diffraction obtained from a ''single-twin domain'' exhibits the well-defined [(2/5)00] and [(3/5)00] diffuse maxima of the O-V phase. The diffraction pattern presented in Ref. 5 does not show the noticeable presence of the [(1/2)00]-type maxima of the O-II phase, that is, the O-V phase seems to be formed by the same mechanism as is suggested above—by the direct transition from the O-I phase under the condition where the formation of the O-II phase is either avoided or suppressed. The diffraction from the O-V order was reported also in Refs. 7 and 26. The very fact that, in spite of all difficulties, several studies nevertheless did observe the [(2/5)00] and [(3/5)00] diffuse maxima is an indication that the O-V phase is stable (or at least metastable) at low temperatures. The ability of our ordering model to predict formation of the O-V phase as a stable state at $x\sim 3/5$ and $T\sim T_{\text{room}}$ suggests that this model describes the system reasonably well.

4. $2\sqrt{2}a_0\times 2\sqrt{2}a_0$ *phases*

The $2\sqrt{2}a_0\times 2\sqrt{2}a_0$ and $\sqrt{2}a_0\times 2\sqrt{2}a_0$ ordered phases [or the {(1/4)(1/4)0} phases, named so after positions of their generic superlattice spots] are known to appear mostly in the substoichiometric region, $x<x_{\text{cr}}\sim 0.35$–0.4.[2,3,5–9,11–13] In this region of x, these ordered phases are formed by alternating oxygen atoms chains along the ⟨110⟩ directions. They are the structural derivatives of the $[(1/2)(1/2)0]_2$ primary ordered phase generated by the Lifshitz star [(1/2)(1/2)0] (see Sec. III). These {(1/4)(1/4)0} phases are produced by the sequence of ordering reactions: $T\rightarrow[(1/2)(1/2)0]_2\rightarrow[(1/4)(1/4)0]_2\rightarrow[(1/4)(1/4)0]_1$. The structural and thermodynamic analysis of these {(1/4)(1/4)0} phases formed at $x<0.4$ was given in our previous study.[14]

However, the [(1/4)(1/4)0]-type diffraction spots were also observed[2–4] within the stoichiometry range $x>0.5$ which is discussed in this study. There is still a question whether the [(1/4)(1/4)0]-type diffraction spots observed in Refs. 2–4 are really generated by the phases at $x>0.5$, as is stated in these works, or they are associated with stoichiometry heterogeneities, being generated by oxygen poor regions with $x<0.4$ imbedded into the matrix with $x>0.5$. The ordering model presented in this paper may clarify some aspects of this problem. In particular, the computer simulation of ordering can show (i) whether the adopted interaction model provides the $2\sqrt{2}a_0\times 2\sqrt{2}a_0$ ordering and the atomic arrangement corresponding to this ordering, (ii) what is the stability range of this structure, and (iii) if the $2\sqrt{2}a_0\times 2\sqrt{2}a_0$ phase is really stable, what kind of kinetics provides its formation.

The computer-simulation picture of the ordered structure developed in a ''quenched'' large domain of the O-II phase at $x=3/4$ is presented in Fig. 6. It does show that ordering produces the $2\sqrt{2}a_0\times 2\sqrt{2}a_0$ order and indicates the atomic structure of this phase. Comparison of the free energies of the obtained $2\sqrt{2}a_0\times 2\sqrt{2}a_0$ structure, the O-I, O-II, and O-III phases given in Fig. 3(c) demonstrates that the $2\sqrt{2}a_0\times 2\sqrt{2}a_0$ phase is stable between approximately 30 and 40 °C.

The O-II→$2\sqrt{2}a_0\times 2\sqrt{2}a_0$ ordering kinetics easily occurs in a *large* domain of the O-II phase (Fig. 6) since there is no size effect preventing this ordering and since the symmetry of the $2\sqrt{2}a_0\times 2\sqrt{2}a_0$ phase is a subgroup of the symmetry of the O-II phase. However, formation of the $2\sqrt{2}a_0\times 2\sqrt{2}a_0$ phase at $x\sim 3/4$ can hardly be expected if the O-II phase at this composition forms fine microdomains. Our computer simulation confirms this conclusion. On the other hand, the presented study confirms our previous results[19,20,22] that (i) the [(1/4)(1/4)0]-type diffuse maxima of the $2\sqrt{2}a_0\times 2\sqrt{2}a_0$ ordered phase are easily formed upon cooling or quenching the O-I microtwins, the (110) twin-related orientation variants of the O-I phase, and (ii) the (110) twin boundaries serve as nucleation sites of the $2\sqrt{2}a_0\times 2\sqrt{2}a_0$ phase facilitating its formation.

A special role played by the {110} twins in the direct O-I→$2\sqrt{2}a_0\times 2\sqrt{2}a_0$ ordering is associated with the following factors. This ordering is the first-order transition. It requires a nucleation and the (110) twin boundaries are its natural nucleation sites under the condition of a weak driving force. The (110) twin boundary promotes the concentration wave whose front is parallel to the (110) twin plane and thus whose wave vector **k** is parallel to the direction [110] perpendicular the the twin plane. The length of the vector **k** falls near the [(1/4)(1/4)0] point which is also located on the same [110] direction. This coincidence seems to be responsible for

potency of the (110) twin boundaries as the nucleation sites. The (110) twin boundaries result in ordering generating a pair of the $\pm[(1/4)(1/4)0]$ superlattice spots, while the (110) twin boundaries result in ordering generating the other pair of the $\pm[(1/4)(1/4)0]$ spots. Since the parent O-I phase, as a rule, is formed as an aggregate of the (110) and (110) twins, which accommodate the elastic strain caused by the orthorhombicity of the O-I phase, the ordering produces all four $\{(1/4)(1/4)0\}$ generic diffraction spots.

The computer-simulated microstructure and the corresponding diffraction pattern obtained by quenching the (110) twins of the O-I phase at $x=3/4$ are presented in Fig. 7. Figure 7 shows small domains of $2\sqrt{2}a_0\times 2\sqrt{2}a_0$ phase in two twin-related orientation variants and their two sharp and strong $\pm[(1/4)(1/4)0]$ superlattice spots located on the direction perpendicular to the twinning plane. The sharpness of these spots is in agreement with the sharpness of the observed $\{(1/4)(1/4)0\}$-type diffraction maxima. The latter is always emphasized by researchers because of the striking contrast with wide and weak [(1/2)00]-type maxima of the O-II phase which are usually observed in this system, even at $x\sim 0.5$.[15,17]

Therefore, our computer simulation suggests that the $\{(1/4)(1/4)0\}$-type sharp maxima of the $2\sqrt{2}a_0\times 2\sqrt{2}a_0$ phase observed at $x>0.5$ in Refs. 2–4 are probably associated with the effect of the (110) twin boundaries of the parent O-I phase and that the presence of twin boundaries extends the temperature and stoichiometry field, where the $2\sqrt{2}a_0\times 2\sqrt{2}a_0$ order may appear, beyond its thermodynamic stability field around $x\sim 3/4$ and $T\sim 30$ °C.

It should be also noted that the $\{(1/4)(1/4)0\}$ phases formed at $x<0.4$, i.e., on other side of the critical concentration $x_{cr}\sim 0.35$, have a different formation mechanism and different structures.[14]

ACKNOWLEDGMENTS

We gratefully acknowledge the support by Division of Materials Science, U.S. Department of Energy, under Grant No. DE-FG05-90ER45430. The simulation was performed on CRAY C-90 at the Pittsburgh Supercomputing Center under Grant No. DMR910002P. One of the authors (A.K.) is grateful to the Institute for Mechanics and Materials Science at the University of California at San Diego where part of this work was done.

APPENDIX: STRAIN-INDUCED INTERACTION

The strain-induced interaction $W(\mathbf{r}-\mathbf{r}')_{pq}^{\text{elast}}$ in Eq. (3) is defined exactly in the same form as in Ref. 14. Its Fourier transform

$$V^{\text{el}}(\mathbf{k})_{pq}=\sum_{\mathbf{r}} W(\mathbf{r})_{pq}^{\text{elast}}\exp(-i\mathbf{kr})$$

can be expressed through the phonon Green function $G(\mathbf{k})_{ij}$ and the Fourier transform $\mathbf{F}_p(\mathbf{k})$ of Kanzaki force $\mathbf{F}_p(\mathbf{r}-\mathbf{r}')$ characterizing the interaction of a Cu atom located in a site $\mathbf{r}$ with an oxygen atom in a site $(p,\mathbf{r}')$:

$$V^{\text{el}}(\mathbf{k})_{pq}=-F_p(\mathbf{k})_i G(\mathbf{k})_{ij} F_q^*(\mathbf{k})_j, \tag{A1}$$

where the nonvanishing components of the Green function tensor $G(\mathbf{k})_{ij}$ in the xy plane can be expressed through the nonzero components of the elastic moduli tensor c_{ijkl} for the tetragonal disordered host lattice, $c_{xxxx}=c_{yyyy}=c_{11}$, $c_{xxyy}=c_{12}$, and $c_{xyxy}=c_{66}$,

$$\begin{aligned}
G(\mathbf{k})_{xx}&=4c[c_{11}\sin^2\pi k+c_{66}\sin^2\pi h]D(h,k)^{-1},\\
G(\mathbf{k})_{yy}&=4c[c_{11}\sin^2\pi h+c_{66}\sin^2\pi k]D(h,k)^{-1},\\
G(\mathbf{k})_{xy}&=-c[(c_{12}+c_{66})\ \sin 2\pi h\ \sin 2\pi k]D(h,k)^{-1},
\end{aligned} \tag{A2}$$

where

$$D(h,k)=c^2[16(c_{11}\sin^2\pi h+c_{66}\sin^2\pi k)(c_{11}\sin^2\pi k+c_{66}\sin^2\pi h)-[(c_{12}+c_{66})\sin 2\pi h\ \sin 2\pi k]^2],$$

$\mathbf{k}=(2\pi/a_0)(h,k)$, h and k are the coordinates of $\mathbf{k}$ within the first Brillouin zone of the host lattice, a_0 and c are the parameters of this lattice (translations along the [100] and [001] directions).

If only the nearest- and next-nearest-neighbor interaction terms are used to calculate the Kanzaki forces, the latter can be expressed in terms of the macroscopic constants by the long-wave transition in the Fourier transform $F_p(\mathbf{k})$ of the Kanzaki forces. These constants are the elastic constants c_{ij}, the lattice parameters a,b,c of the orthorhombic lattice of $YBa_2Cu_3O_7$ and the parameters of the $YBa_2Cu_3O_6$ tetragonal lattice a_0, c_0. Details of this procedure are presented in Ref. 29. The result is

$$\begin{aligned}
F_1(\mathbf{k})&=-ia_0c_0\epsilon_0(c_{11}-c_{12})\exp\left(i\frac{\mathbf{ka}}{2}\right)[f_x,f_y],\\
F_2(\mathbf{k})&=-ia_0c_0\epsilon_0(c_{11}-c_{12})\exp\left(i\frac{\mathbf{kb}}{2}\right)[v_x,v_y],
\end{aligned} \tag{A3}$$

where $\epsilon_0=(b-a_0/a_0)$ and

$$\begin{aligned}
f_x&=2.25\sin\left(\frac{\mathbf{ka}}{2}\right)-0.25\sin\left(\frac{\mathbf{ka}}{2}\right)\cos(\mathbf{kb}),\\
f_y&=-\sin(\mathbf{kb})\cos\left(\frac{\mathbf{ka}}{2}\right),
\end{aligned}$$

$$v_x = -\sin(\mathbf{ka})\cos\left(\frac{\mathbf{kb}}{2}\right),$$

$$v_y = 2.25\,\sin\left(\frac{\mathbf{kb}}{2}\right) - 0.25\,\sin\left(\frac{\mathbf{kb}}{2}\right)\cos(\mathbf{ka}), \qquad \text{(A4)}$$

with $\mathbf{ka}=2\pi h$, $\mathbf{kb}=2\pi k$.

All parameters in Eqs. (A2)–(A4) are obtained from the following data:

$$a = 3.822\ \text{Å},\ b = 3.891\ \text{Å},\ c = 11.677\ \text{Å}\ \ (\text{Ref. } 37),$$

$$c_{11} \sim 2.3\times 10^{12},$$

$$c_{12} \sim 1.0\times 10^{12},$$

$$c_{66} \sim 0.85\times 10^{12}\ \ (\text{in dn/cm}^2)\ \ (\text{Ref. } 38). \qquad \text{(A5)}$$

The parameter ϵ_0 is found by using values (A5) and the estimate $a_0(a+b)/2 = 3.856$Å in definition $\epsilon_0 = (b-a_0)/a_0$. It gives $\epsilon_0 \sim 0.009$.

[1] A. G. Khachaturyan and J. W. Morris, Jr., Phys. Rev. Lett. **61**, 215 (1988).

[2] M. A. Alario-Franco, J. J. Capponi, C. Chaillout, and J. Chenavas, in *High Temperature Superconductor*, edited by M. B. Brodsky, R. C. Dynes, K. Kilazawa, and H. L. Tuller, MRS Symposia Proceedings No. 99 (Materials Research Society Pittsburgh, 1988), p. 41.

[3] M. A. Alario-Franco, C. Chaillout, J. J. Capponi, J. Chenavas, and M. Marezio, Physica C **156**, 455 (1988).

[4] R. J. Cava, A. W. Hewat, E. A. Hewat, B. Batlogg, M. Marezio, K. M. Rabe, J. J. Krajewski, W. F. Peck, Jr., and L. W. Rupp, Jr., Physica C **165**, 419 (1990).

[5] M. A. Alario-Franco, C. Chaillout, J. J. Capponi, and J. Chenavas, Mater. Res. Bull. **22**, 1685 (1987).

[6] C. Chaillout, M. A. Alario-Franco, J. J. Capponi, J. Chenavas, J. L. Hodeau, and M. Marezio, Phys. Rev. B **36**, 7118 (1987).

[7] J. Reyes-Gasga, T. Krekels, G. Van Tendeloo, J. Van Landuyt, S. Amelinckx, W. H. M. Bruggink, and H. Werweij, Physica C **159**, 831 (1989).

[8] Tan Kemin, Hu Meisheng, and W. Yening, J. Phys. Condens. Matter **1**, 1049 (1989).

[9] T. Krekels, T. S. Shi, J. Reyes-Gasga, G. Van Tendello, J. Van Landuyt, and S. Amelinckx, Physica C **167**, 677 (1990).

[10] D. J. Werder, C. H. Chen, and G. P. Espinosa, Physica C **173**, 285 (1991).

[11] R. Sonntag, D. Hohlwein, T. Brucke, and G. Collin, Phys. Rev. Lett. **66**, 1497 (1991).

[12] R. Sonntag, Th. Zeiske, and D. Hohlwein, Physica B **180–181**, 374 (1992).

[13] Th. Zeiske, D. Hohlwein, R. Sonntag, F. Kubanek, and G. Collin, Z. Phys. B **86**, 11 (1992).

[14] S. Semenovskaya and A. G. Khachaturyan, Phys. Rev. B **51**, 8409 (1995).

[15] W. Schwartz, O. Blaschko, G. Collin, and F. Marucco, Phys. Rev. B **48**, 6513 (1993).

[16] S. Yang, H. Claus, B. W. Veal, R. Wheeler, A. P. Paulikas, and J. W. Downey, Physica C **193**, 243 (1992).

[17] Th. Zeiske, R. Sonntag, D. Hohlwein, N. H. Andersen, and T. Wolf, Nature **353**, 542 (1991).

[18] S. Semenovskaya and A. G. Khachaturyan, Phys. Rev. Lett. **67**, 2223 (1991).

[19] S. Semenovskaya and A. G. Khachaturyan, Phys. Rev. B **46**, 6511 (1992).

[20] S. Semenovskaya and A. G. Khachaturyan, Physica D **66**, 205 (1993).

[21] S. Semenovskaya, Y. Zhu, M. Suenaga, and A. G. Khachaturyan, Phys. Rev. B **47**, 12 182 (1993).

[22] S. Semenovskaya and A. G. Khachaturyan, Philos. Mag. Lett. **66**, 105 (1992).

[23] V. Plakhty, A. Stratilatov, Yu. Chernenkov, V. Fedorov, S. K. Sinha, C. L. Loong, B. Gaulin, M. Vlasov, and S. Moshkin, Solid State Commun. **84**, 639 (1992).

[24] B. W. Veal, A. P. Paulikas, Hoydoo You, Hao Shi, Y. Fang, and J. W. Downey, Phys. Rev. B **42**, 6305 (1990).

[25] D. J. Werder, C. H. Chen, R. J. Cava, and B. Batlogg, Phys. Rev. B **37**, 2317 (1988).

[26] R. Beyers, B. T. Ahn, G. Gorman, V. Y. Lee, S. S. P. Parkin, M. L. Ramirez, K. P. Roche, J. E. Vazquez, T. M. Gur, and R. A. Huggins, Nature **340**, 6235 (1989).

[27] A. G. Khachaturyan and B. I. Pokrovskii, in *Progress in Materials Science*, edited by J. W. Christian, P. Haasen, and T. Massalski (Pergamon, Oxford, 1985), Vol. 29, pp. 1–138.

[28] A. G. Khachaturyan, Phys. Status Solidi B **60**, 9 (1973); Sov. Phys.-JETP **36**, 753 (1973).

[29] A. G. Khachaturyan, *The Theory of Structural Transformation in Solids* (Wiley, New York, 1983).

[30] A. A. Aligia, J. Garces, and H. Bonadeo, Physica C **190**, 234 (1992).

[31] A. A. Aligia and J. Garces, Solid State Commun. **87**, 363 (1993).

[32] A. A. Aligia and J. Garces, Phys. Rev. B **49**, 524 (1994).

[33] D. Adelman, C. P. Burmester, L. T. Willi, P. A. Stern, and R. Gronsky, J. Phys. Condens. Matter **4**, L585 (1992).

[34] J. D. Jorgensen, M. A. Beno, D. G. Hinks, L. Soderholm, H. J. Volin, R. L. Hitterman, J. D. Grace, I. K. Schuller, C. V. Segre, K. Zhang, and M. S. Kleefish, Phys. Rev. B **36**, 3608 (1987).

[35] S. Semenovskaya, Phys. Status Solidi B **64**, 291 (1974).

[36] J. D. Jorgensen, B. W. Veal, A. P. Paulikas, L. J. Nowicki, G. W. Crabtree, H. Claus, and W. K. Kwok, Phys. Rev. B **41**, 1863 (1990).

[37] R. J. Cava, B. Batlogg, C. H. Chen, E. A. Reitman, S. M. Zahurak, and D. Werder, Nature **329**, 423 (1987).

[38] Ming Lei, J. L. Sarrao, W. M. Visscher, T. M. Bell, J. D. Thompson, A. Migliori, U. W. Welp, and B. Veal, Phys. Rev. B **47**, 6154 (1993).